Monthly Notices
of the
ROYAL ASTRONOMICAL SOCIETY

Mon. Not. R. Astron. Soc. **419,** 827–840 (2012) doi:10.1111/j.1365-2966.2011.19747.x

Nuclear-dominated accretion and subluminous supernovae from the merger of a white dwarf with a neutron star or black hole

B. D. Metzger★†

Department of Astrophysical Sciences, Peyton Hall, Princeton University, Princeton, NJ 08544, USA

Accepted 2011 September 1. Received 2011 August 9; in original form 2011 May 30

ABSTRACT

We construct one-dimensional steady-state models of accretion discs produced by the tidal disruption of a white dwarf (WD) by a neutron star (NS) or stellar mass black hole (BH). At radii $r \lesssim 10^{8.5}$–10^{9} cm the mid-plane density and temperature are sufficiently high to burn the initial WD material into increasingly heavier elements (e.g. Mg, Si, S, Ca, Fe and Ni) at sequentially smaller radii. When the energy released by nuclear reactions is comparable to that released gravitationally, we term the disc a nuclear-dominated accretion flow (NuDAF). At small radii $\lesssim 10^{7}$ cm iron photodisintegrates into helium and then free nuclei, and in the very innermost disc cooling by neutrinos may be efficient. At the high accretion rates of relevance $\sim 10^{-4}$ to $0.1\,\mathrm{M}_{\odot}\,\mathrm{s}^{-1}$, most of the disc is radiatively inefficient and prone to outflows powered by viscous dissipation and nuclear burning. Outflow properties are calculated by requiring that material in the mid-plane be marginally bound (Bernoulli constant $\lesssim 0$), due (in part) to cooling by matter escaping the disc. For reasonable assumptions regarding the properties of disc winds, we show that a significant fraction ($\gtrsim$ 50–80 per cent) of the total WD mass is unbound. The composition of the ejecta is predominantly O, C, Si, Mg, Ne, Fe and S [He, C, Si, S, Ar and Fe], in the case of C–O [pure He] WDs, respectively, along with a small quantity $\sim 10^{-3}$ to $10^{-2}\,\mathrm{M}_{\odot}$ of radioactive ^{56}Ni and, potentially, a trace amount of hydrogen. Depending on the pressure dependence of wind cooling, we find that the disc may be thermally unstable to nuclear burning, the likelihood of which increases for higher mass WDs. We use our results to evaluate possible electromagnetic counterparts of WD–NS/BH mergers, including optical transients powered by the radioactive decay of ^{56}Ni and radio transients powered by the interaction of the ejecta with the interstellar medium. We address whether recently discovered subluminous Type I supernovae result from WD–NS/BH mergers. Ultimately assessing the fate of these events requires global simulations of the disc evolution, which capture the complex interplay between nuclear burning, convection and outflows.

Key words: accretion, accretion discs – nuclear reactions, nucleosynthesis, abundances – supernovae: general – white dwarfs.

1 INTRODUCTION

Sensitive wide-field optical surveys are revolutionizing our understanding of time-dependent astrophysical phenomena. New types of stellar explosions, which were once too faint or rare to be detected, are now routinely discovered by efforts such as the Palomar Transient Factory (Law et al. 2009; Rau et al. 2009) and Panoramic Survey Telescope and Rapid Response System (PanSTARRs) (Kaiser et al. 2002). As our census of the transient universe expands, it becomes increasingly important to evaluate the expected (EM) counterparts of known astrophysical events.

Several Type I supernovae (SNe I) have recently been discovered, which are dimmer and/or more rapidly evolving than normal SNe Ia or Ib/c. Included among these is a class of peculiar SNe Ia characterized by lower luminosities and lower ejecta velocities than normal SNe Ia ('SN 2002cx-like events'; Li et al. 2003; Jha et al. 2006), and which occur predominantly in star-forming galaxies (Foley et al. 2009). SN 2008ha is an extreme example, with a peak brightness and rise time of only $M_{\mathrm{V}} \simeq -14$ and $\sim$10 d, respectively (Foley et al. 2009, 2010; Valenti et al. 2009). Another recently identified class of subluminous transients are SNe Ib with Ca-rich [but S-, Si- and Fe-poor] spectra (e.g. SN 2005e; Perets et al. 2010). These events appear to result from ejecta that have undergone helium burning (Perets et al. 2010, 2011; Waldman et al. 2011) and, unlike 2002cx-like events, are associated with an older

★E-mail: bmetzger@astro.princeton.edu
†NASA Einstein Fellow.

stellar population located in the outskirts of their host galaxies. Even more rapidly evolving SNe such as 2002bj (Poznanski et al. 2010) and 2010X (Kasliwal et al. 2010) may be related to this class.

Lacking hydrogen in their spectra, SNe I are generally thought to originate from compact progenitors such as white dwarfs (WDs) or massive stars without extended envelopes. Because compact stars lose most of their initial thermal energy to adiabatic expansion during the explosion, their emission must be powered by continued energy input from the radioactive decay of isotopes such as ^{56}Ni. The rapid evolution and low luminosities of events like 2002cx and 2005E thus require both a significantly lower ^{56}Ni yield, and total ejecta mass, than characterize normal SNe.

It is economical to associate new classes of SNe with anticipated variations of well-studied models, such as the core collapse of a massive star or the thermonuclear explosion of a WD. Events like 2002cx may, for instance, result from the pure deflagration of a Chadrasekhar or sub-Chandrasekhar mass WD (e.g. Branch et al. 2004; Phillips et al. 2007), as opposed to the 'delayed detonation' models that best describe normal SNe Ia (Nomoto, Thielemann & Yokoi 1984). They may alternatively result from weak core collapse explosions (Valenti et al. 2009; Moriya et al. 2010). For Ca-rich SNe Ib like 2005E, a promising explanation is the detonation of a helium shell on the surface of a C/O WD (Woosley, Taam & Weaver 1986; Iben & Tutukov 1991; Livne & Arnett 1995; Bildsten et al. 2007; Shen et al. 2010; Woosley & Kasen 2011). Though promising, none of these explanations is yet definitive (e.g. Woosley & Kasen 2011). The possibility thus remains that at least some of these events represent an entirely new type of stellar explosion.

In this paper we examine the observable signatures of the merger of a WD with a binary neutron star (NS) or black hole (BH) companion. Four Galactic WD–NS binaries are currently known, which will merge due to the emission of gravitational radiation within a Hubble time (see Section 2). If mass transfer following Roche lobe overflow (RLOF) is unstable, then the WD is tidally disrupted, producing a massive disc around the NS or BH. Past work has focused on the possibility that accretion powers a relativistic jet and a gamma-ray burst (Fryer et al. 1999; King, Olsson & Davies 2007a). Here we instead focus on the properties of the accretion flow on larger scales. We address two aspects of the problem neglected in previous studies: (1) the presence of (non-relativistic) outflows from the disc and (2) the effects of nucleosynthesis on the thermodynamics and composition of the disc and outflows. Although multidimensional numerical simulations are ultimately necessary to evaluate the evolution and fate of these systems, the large range in spatial and temporal scales involved make such a study numerically challenging. Here, as a first step, we instead construct a simplified model of the disc and its outflows that we believe captures some of the essential physics. We use our results for the mass, velocity and composition of the ejecta to quantify the associated EM counterparts of WD–NS/BH mergers for a wide range of systems.

This paper is organized as follows. In Section 2 we discuss the conditions for unstable mass transfer in WD–NS and WD–BH binaries and motivate the initial conditions for our subsequent calculations. In Section 3 we describe one-dimensional steady-state models of the accretion disc and its outflows. In Section 4 we present our results for the disc structure (Section 4.1) and outflow properties (Section 4.2). In Section 4.3 we assess the stability of our solutions and in Section 4.4 we discuss the effects of convection. In Section 5 we use our results to evaluate possible EM counterparts of WD–NS/WD–BH mergers, including subluminous SNe I (Section 5.2) and radio transients (Section 5.3). We conclude in Section 6.

2 UNSTABLE MASS TRANSFER AND DISC FORMATION

A standard scenario for the formation of tight WD–NS/BH binaries invokes common envelope evolution of an initially wide binary, consisting of a NS or BH and an intermediate-mass $\lesssim 8$–$10\,M_\odot$ main-sequence companion (e.g. van den Heuvel & Bonsdema 1984). For a limited range of orbital periods, unstable RLOF begins only after the secondary has left the main sequence. Depending on the evolutionary state of the stellar core when this occurs, the end result is a NS or BH in orbit with a WD with either (from lowest to highest WD mass) a pure He, He–C–O ('hybrid'), C–O or O–Ne composition. Close WD–NS/BH binaries can alternatively form directly by collisions in dense stellar regions, such as the centres of galaxies or globular clusters (Sigurdsson & Rees 1997).

After the WD–NS/BH binary is brought close together, the system continues to lose angular momentum on a longer time-scale to gravitational wave emission. Angular momentum losses may be enhanced by the eccentricity induced by Kozai oscillations if a tertiary companion is present (Thompson 2010). Of the $\gtrsim$20 WD–NS binaries identified in our Galaxy (Lorimer 2005), only four are sufficiently compact that they will merge in $\lesssim 10^{10}$ yr (PSR J0751+1807 – Kaspi et al. 2000; PSR J1757−5322 – Edwards & Bailes 2001; PSR J1141−6545 – Lundgren, Zepka & Cordes 1995; PSR J1738−0333 – Freire & Wex 2010; see O'Shaughnessy & Kim 2010 for a recent compilation). The WD masses in these systems are $M_{\rm WD} = 0.18$, 0.67, 0.99 and $0.2\,M_\odot$, respectively (e.g. Bailes et al. 2003). From the first three of these systems, Kim et al. (2004) estimate that the WD–NS merger rate in the Milky Way is 10^{-6} to 10^{-5} yr^{-1}, although correcting for pulsar beaming increases this rate by a factor of several. Population synthesis models predict somewhat higher rates $\sim 10^{-5}$ to 10^{-3} yr^{-1}, but with larger uncertainty (Portegies Zwart & Yungelson 1999; Tauris & Sennels 2000; Davies, Ritter & King 2002). No confirmed WD–BH systems are currently known.

Once the orbital period decreases to $\lesssim$1 min, the WD undergoes RLOF on to the NS/BH companion. Approximating the WD as a $\Gamma = 5/3$ polytrope, its radius is

$$R_{\rm WD} \simeq 10^4 \left(\frac{M_{\rm WD}}{0.7\,M_\odot}\right)^{-1/3} \left[1 - \left(\frac{M_{\rm WD}}{M_{\rm ch}}\right)^{4/3}\right]^{1/2} \left(\frac{\mu_{\rm e}}{2}\right)^{-5/3} {\rm km}, \quad (1)$$

where $M_{\rm ch} = 1.4\,M_\odot$ and $\mu_{\rm e}$ is the mean molecular weight per electron (Nauenberg 1972). The orbital separation at Roche contact is approximately (Eggleton 1983)

$$R_{\rm RLOF} = R_{\rm WD} \frac{0.6q^{2/3} + \ln(1+q^{1/3})}{0.49q^{2/3}}, \quad (2)$$

where $q = M_{\rm WD}/M$ and M is the mass of the primary BH or NS.

If orbital angular momentum is conserved, then mass transfer is unstable for $q \gtrsim 0.4$–0.55 (e.g. Verbunt & Rappaport 1988; see Paschalidis et al. 2009, their fig. 11). If strictly applicable, this criterion would limit tidal disruption to NS binaries with relatively massive $\gtrsim 0.5\,M_\odot$ C–O/O–Ne WDs, and might preclude disruption in WD–BH binaries altogether. Stable systems increase their orbital separation after mass transfer begins. The result is a long-lived accreting system, which may be observed as an ultracompact X-ray binary (e.g. Verbunt & van den Heuvel 1995).

Conservative mass transfer is, however, unlikely. Tidal coupling during inspiral can transfer orbital angular momentum into spin. Furthermore, the accretion rate on to the NS/BH just after RLOF is highly super-Eddington, in which case a common envelope may

engulf the system and outflows are likely (e.g. Ohsuga et al. 2005). Depending on the amount of angular momentum lost to winds or tides, unstable mass transfer may occur in systems with even lower mass ratios $q \lesssim 0.3$ (e.g. Yungelson, Nelemans & van den Heuvel 2002). In this case, tidal disruption may occur also for NS binaries with He or 'hybrid' He–C–O WD companions, or even in the case of C–O/O–Ne WDs with low mass $\sim 3\,\mathrm{M}_\odot$ BHs (Fryer et al. 1999). Future numerical simulations are required to address the challenging issue of stability in degenerate binary mergers (e.g. Guerrero, García-Berro & Isern 2004; D'Souza et al. 2006).

If mass transfer is unstable, then the WD is tidally disrupted in just a few orbits. The WD material then circularizes and produces a disc around the central NS/BH with a total mass $M_{\rm WD}$ and characteristic radius $R_{\rm d} \sim R_{\rm RLOF}(1+q)^{-1}$. This disc accretes on to the NS/BH on the viscous time-scale

$$t_{\rm visc} \simeq \alpha^{-1}\left(\frac{R_{\rm d}^3}{GM}\right)^{1/2}\left(\frac{H}{R_{\rm d}}\right)^{-2} \sim 140\,{\rm s}\left(\frac{\alpha}{0.1}\right)^{-1}\left(\frac{M}{1.4\,\mathrm{M}_\odot}\right)^{-1/2}\left(\frac{R_{\rm d}}{10^9\,{\rm cm}}\right)^{3/2}\left(\frac{H/R_{\rm d}}{0.4}\right)^{-2} \quad (3)$$

and at a characteristic rate

$$\dot{M}(R_{\rm d}) \sim \frac{M_{\rm WD}}{t_{\rm visc}} \sim 10^{-2}\,\mathrm{M}_\odot\,{\rm s}^{-1}\left(\frac{\alpha}{0.1}\right)\left(\frac{M}{1.4\,\mathrm{M}_\odot}\right)^{1/2} \times \left(\frac{M_{\rm WD}}{0.7\,\mathrm{M}_\odot}\right)\left(\frac{R_{\rm d}}{10^9\,{\rm cm}}\right)^{-3/2}\left(\frac{H/R_{\rm d}}{0.4}\right)^{2}, \quad (4)$$

where M is the NS/BH mass, α parametrizes the disc viscosity (Section 3), and H is the scaleheight of the disc, normalized to a characteristic value (Section 4). Turbulence in the disc is driven by the magnetorotational instability, which transports angular momentum at a rate corresponding to $\alpha \sim 0.01$–0.1 (e.g. Davis, Stone & Pessah 2010). Because the mass of the disc is significant compared to that of the central NS or BH, the disc may also be gravitationally unstable, which likely results in even more efficient angular momentum transport (e.g. Laughlin & Bodenheimer 1994). In Section 4.4 we describe how the disc lifetime is altered if convection plays an important role in transporting angular momentum.

Applying equations (2) and (4) to the full range of unstable systems, we conclude that the majority of the WD mass accretes at a rate $\dot{M}(R_{\rm d}) \sim 10^{-4}$ to $10^{-1}\,\mathrm{M}_\odot\,{\rm s}^{-1}$, depending primarily on $M_{\rm WD}$ and α. More massive WDs accrete at a higher rate, because both $\dot{M} \propto R_{\rm d}^{-3/2} \propto R_{\rm RLOF}^{-3/2}(1+q)^{3/2}$ and possibly α (if the disc is gravitationally unstable) increase with q. At such high accretion rates ($\sim 10^{11}$–10^{14} times larger than the Eddington rate) the disc cannot cool through photon emission and is termed a radiatively inefficient accretion flow (RIAF).

3 ACCRETION DISC AND OUTFLOW MODEL

In this section we present a one-dimensional steady-state model of the accretion discs produced by WD–NS/BH mergers. Although the steady-state approximation is clearly invalid just after the merger, it represents a reasonable description on time-scales $\sim t_{\rm visc}$, during which most of the mass accretes at the rate estimated in equation (4). We address the stability of our solutions in Section 4.3.

We adopt a height-integrated model, motivated by previous work on RIAFs in the context of 'advection-dominated' models (Narayan & Yi 1994) with outflows (Narayan & Yi 1995; Blandford & Begelman 1999). Because RIAFs are geometrically thick, averaging over the vertical structure serves only as a crude approximation. In standard RIAF models, viscous heating is balanced by advective cooling, due either to accretion or outflows (see Narayan, Mahadevan & Quataert 1998, for a review). As we describe below, a key aspect of accretion following WD–NS/BH mergers is the relative importance of heating from nuclear reactions compared to viscous heating. We term this novel accretion regime a nuclear-dominated accretion flow (NuDAF).

We begin by defining the (positive) steady-state accretion rate

$$\dot{M}(r) \equiv -2\pi r \Sigma v_r, \quad (5)$$

where $\Sigma = 2H\rho$ is the surface density, ρ is the mid-plane density, H is the vertical scaleheight and $v_r < 0$ is the radial velocity. We allow for the presence of a wind with a mass-loss rate $\dot{M}_{\rm w}$, which we characterize by the local quantity

$$p(r) \equiv \frac{\partial \ln \dot{M}_{\rm w}}{\partial \ln r}. \quad (6)$$

We do not demand that $p(r)$ be constant with radius, but rather determine its functional form self-consistently from the solution, as described below.

We assume that the wind exerts no torque on the disc, such that it carries away only its own specific angular momentum, i.e. $j_{\rm w} = j_{\rm d} = r^2\Omega$, where Ω is the angular velocity. This is valid provided that the disc is not threaded by a large-scale field of sufficient strength to establish an Alfvén radius significantly above the disc surface. We furthermore assume that no torque is applied by the inner boundary, such that (at radii much greater than the inner disc edge) the radial velocity obeys

$$v_r \simeq \frac{\nu}{\Omega}\frac{\partial \Omega}{\partial r} \approx -\frac{3}{2}\frac{\nu}{r} = -\frac{3}{2}\alpha\left(\frac{H}{r}\right)^2 v_{\rm k}, \quad (7)$$

where we adopt a Shakura & Sunyaev (1973) kinematic viscosity $\nu = \alpha P/\rho\Omega$ with $\alpha \ll 1$; $H \approx a/\Omega < r$ is the vertical scaleheight; $a \equiv (P/\rho)^{1/2}$ defines the mid-plane sound speed; and in the last expression we assume that Ω equals the Keplerian rate $\Omega_{\rm k} = (GM/r^3)^{3/2} = v_{\rm k}/r$ to leading order in $(H/r)^2$. In adopting an anomalous viscosity we have implicitly assumed that angular momentum by magnetohydrodynamics (MHD) turbulence or gravitational instability *outwards* dominates any *inward* transport from convection; in Section 4.4 we discuss the validity of this point. From equation (5) we note that $\dot{M} = 3\pi\nu\Sigma$.

Mass continuity $\partial\dot{M}_{\rm d}/\partial r = \partial\dot{M}_{\rm w}/\partial r$ implies that

$$\frac{\partial \ln \rho}{\partial \ln r} + 3\frac{\partial \ln a}{\partial \ln r} = p - 3, \quad (8)$$

while radial momentum conservation

$$v_r\frac{\partial v_r}{\partial r} + \frac{1}{\rho}\frac{\partial P}{\partial r} + \frac{GM}{r^2} - r\Omega^2 = 0 \quad (9)$$

requires that

$$\frac{\partial \ln \rho}{\partial \ln r} + 2\frac{\partial \ln a}{\partial \ln r} - \frac{r^2\left(\Omega^2 - \Omega_{\rm k}^2\right)}{a^2} = 0, \quad (10)$$

where we have neglected the first term $\propto v_r^2 \propto (H/r)^4$.

The entropy equation reads

$$\dot{q}_{\rm adv} \equiv v_r T\frac{\partial s}{\partial r} = v_r\left(\frac{\partial \epsilon}{\partial r} + P\frac{\partial \rho^{-1}}{\partial r}\right) = \frac{v_r a^2}{r}\left(\frac{2}{\gamma - 1}\frac{\partial \ln a}{\partial \ln r} - \frac{\partial \ln \rho}{\partial \ln r}\right) = \dot{q}, \quad (11)$$

where T is the mid-plane temperature, $\gamma \in [4/3, 5/3]$ is the adiabatic index, and s and ϵ are the specific entropy and internal energy, respectively. We have neglected the chemical potential term $\propto \mu_i \partial Y_i/\partial r$ because all species (including electrons) are non-degenerate at the radii where nuclear burning commences. Equation (11) may be interpreted as the balance between 'cooling' from advection through the disc $\dot{q}_{\rm adv}$ and other sources of heating/cooling $\dot{q} = \dot{q}_{\rm visc} + \dot{q}_{\rm nuc} + \dot{q}_{\rm w}$, including those resulting from nuclear reactions $\dot{q}_{\rm nuc}(\rho, T)$ (see equation 14), winds $\dot{q}_{\rm w}$ (see below) and viscous dissipation

$$\dot{q}_{\rm visc} = \nu r^2 \left(\frac{\partial \Omega}{\partial \ln r}\right)^2 \simeq \frac{9}{4}\nu\Omega^2 = \frac{9}{4}\nu\Omega_{\rm k}^2 \left[1 + \left(\frac{H}{r}\right)^2 \left(\frac{\partial \ln \rho}{\partial \ln r} + 2\frac{\partial \ln a}{\partial \ln r}\right)\right], \quad (12)$$

where we have used equation (10) in the last expression and neglect terms $\propto \partial(H/r)/\partial r$. We again note that radiative cooling may be neglected because the time-scale for photon diffusion from the disc mid-plane is much longer than the viscous time (equation 3). In Section 4.4 we describe a scenario in which this might be violated, but this alternative picture of the disc evolution is radically different from the model developed in this section.

An important characteristic of RIAFs without outflows ($p = 0$) is that the Bernoulli parameter

$$\mathrm{Be_d} \equiv \frac{1}{2}v_r^2 + \frac{1}{2}r^2\Omega^2 + \epsilon + \frac{P}{\rho} - \frac{GM}{r} \quad (13)$$

is generically positive (Narayan & Yi 1994). This implies that, in principle, material in the mid-plane has sufficient energy to escape to infinity. This fact has been used previously to argue that RIAFs are susceptible to powerful outflows (Narayan & Yi 1995; Blandford & Begelman 1999) that carry away a substantial portion of the accreting mass, viz. $p \in [0, 1]$. If a fraction of the accreting matter does in fact escape, then the upper atmosphere of the disc must be *preferentially heated*. Only in this manner can the wind achieve a positive Bernoulli parameter $\mathrm{Be_w} = v_{\rm w}^2/2 > 0$, while the remaining disc material is accordingly cooled and remains bound ($\mathrm{Be_d} \lesssim 0$), where $v_{\rm w}$ is the asymptotic velocity of the wind.

Following previous work (e.g. Kohri, Narayan & Piran 2005), we quantify the efficiency of wind heating by a parameter $\eta_{\rm w} \equiv v_{\rm w}^2/2v_k^2$, which equals the ratio of $\mathrm{Be_w}$ to the local gravitational binding energy. This prescription is certainly not unique; for instance, $v_{\rm w}$ could instead scale with the disc sound speed a. Although for our purposes here this distinction is unimportant since v_k and a have similar values, the pressure dependence of wind cooling is different between these cases, which has an important effect on the thermal stability of the disc (Section 4.3).

As we describe below, by demanding that the Bernoulli parameter in the mid-plane $\mathrm{Be_d} \leq 0$ and fixing $\eta_{\rm w}$, this uniquely specifies the wind mass outflow rate $p(r)$ (equation 6). Although we adopt a 'two zone' model (disc + outflow), we do not specify the source of wind heating explicitly.[1] In most of our calculations we adopt values for $\eta_{\rm w} \sim$ few, because a terminal speed of the order of the escape speed is a common feature of thermally driven winds (e.g. Lamers & Cassinelli 1999).

[1] One possible source of coronal heating is the dissipation of MHD waves. Waves may be excited by turbulence due to the magnetorotational instability (MRI) or vertical convection, the latter of which is likely due to the strong temperature dependence of the nuclear heating rate.

If the wind is heated, then the disc necessarily cools at the rate

$$\dot{q}_{\rm w} = -\frac{(v_{\rm w}^2/2 - \mathrm{Be_d})}{2\pi\Sigma r}\frac{\partial M_{\rm d}}{\partial \ln r} = -\frac{3}{2}p(\eta_{\rm w} - \mathrm{Be_d'})\nu\Omega_{\rm k}^2, \quad (14)$$

where $\mathrm{Be_d'} \equiv \mathrm{Be_d}/v_k^2$ is the 'normalized' disc Bernoulli function.

By combining equations (11)–(14) we find that

$$\left(\frac{H}{r}\right)^2 \left[\frac{3\gamma - 1}{\gamma - 1}\frac{\partial \ln a}{\partial \ln r} + \frac{1}{2}\frac{\partial \ln \rho}{\partial \ln r}\right] = -\frac{2}{3}\frac{\dot{q}_{\rm nuc}}{\nu\Omega_k^2} + p(\eta_{\rm w} - \mathrm{Be_d'}) - \frac{3}{2}. \quad (15)$$

Finally, nuclear reactions change the composition of the accreting material according to

$$v_r\frac{\partial X_A}{\partial r} = \dot{X}_A|_P, \quad (16)$$

where X_A is the mass fraction of isotope with mass number A, and $\dot{X}_A|_P$ is the nuclear reaction rate. Equation (16) shows that material burns for approximately the local accretion time-scale $\sim r/v_r$ at any radius. We assume that burning occurs at constant pressure because in general the burning time-scale is long compared to the dynamical time-scale over which vertical pressure balance is established.

We neglect the effects of convective/turbulent mixing in the disc, which may act to smooth radial abundance gradients; mixing could, in principle, be modelled by including an additional term $\propto \nu_{\rm mix}\nabla^2 X_A$ to the right-hand side of equation (16), where $\nu_{\rm mix}$ is the diffusion coefficient. Neglecting mixing is justified as a first approximation because compositional changes typically occur over a radial distance $\gtrsim H$. Studies of the diffusion of passive contaminants in numerical simulations of the MRI furthermore demonstrate that $\nu_{\rm mix} < \nu$ (e.g. Carballido, Stone & Pringle 2005), such that it appears unlikely that burned material will diffuse upstream.

The nuclear reaction rates $\dot{X}_A(\rho, T)$ and nuclear heating rate $\dot{q}_{\rm nuc}(\rho, T)$ in equations (11) and (16) are calculated using a 19-isotope reaction network[2] that includes α capture, heavy nuclei and $(\alpha, p)(p, \alpha)$ reactions (Timmes 1999). The temperature $T(r)$ and adiabatic index $\gamma(r)$ are calculated using a standard equation of state, which includes ideal gas, radiation and degeneracy pressure.

We calculate solutions by integrating equations (8), (15) and (16) from the outer boundary $r = R_{\rm d}$ inwards, in order to obtain $a(r)$, $\rho(r)$ and $X_A(r)$. The wind mass-loss rate $p(r)$ (equation 6) is determined by demanding that the Bernoulli function is regulated by outflows to a fixed value $\mathrm{Be_d'} = -0.2$ to 0 (marginally bound disc). Boundary conditions are determined by fixing the outer accretion rate $\dot{M}_{\rm d}(R_{\rm d})$ (equation 4) and by assuming that the inflowing material reaches a self-similar evolution with $a \propto v_k \propto r^{-1/2}$, such that $\frac{\partial \ln a}{\partial \ln r}|_{R_{\rm d}} = -1/2$.[3] We terminate our solutions at the radius $R_{\rm in} \lesssim 10^7$ cm at which heavy nuclei are photodisintegrated into free nuclei. Interior to this point, neutrinos from the reactions $\mathrm{e^- + p \rightarrow n + \nu_e}$ and $\mathrm{e^+ + n \rightarrow p + \bar{\nu}_e}$ become an important source of cooling (e.g. Narayan, Piran & Kumar 2001; Chen & Beloborodov 2007). Depending on $\dot{M}$ and α, the disc may become radiatively efficient and geometrically thin, such that strong outflows may be suppressed close to the surface of the central NS/BH. Fig. 1 shows a schematic diagram of the structure of the disc and outflows.

[2] See http://www.cococubed.com/code_pages/burn_helium.shtml.

[3] Regardless of the precise outer boundary condition adopted, the self-similar solution is rapidly obtained (Narayan & Yi 1994). Self-similarity is maintained until nuclear burning becomes important, which introduces an additional scale into the problem.

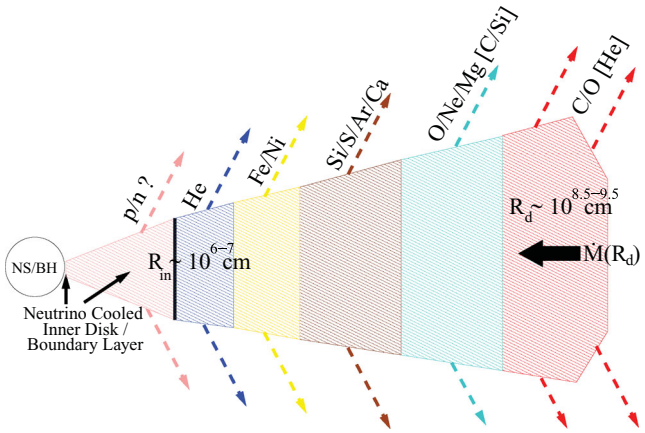

Figure 1. Schematic diagram of accretion and outflows following the merger of a WD–NS/BH binary. At the outer edge of the disc (radius $R_{\rm d} \sim 10^{8.5}$–$10^{9.5}$ cm) the accretion rate $\dot{M}(R_{\rm d})$ is $\sim 10^{-4}$ to $0.1\,{\rm M}_\odot\,{\rm s}^{-1}$, depending on the properties of the merging binary and the viscosity α (equation 4). The outer composition is He, He–C–O, C–O or O–Ne, depending on the properties of the disrupted WD. As matter accretes to small radii, it experiences higher temperatures and burns to increasingly heavier elements. Outflows are driven from the disc (directly or indirectly) by energy released from viscous dissipation and nuclear burning (Figs 2–5). Elements synthesized near the mid-plane are transported to the surface, such that the local composition of the wind matches that of the mid-plane. The outflow composition characterizing each range of radii are shown next to the outgoing arrows for the case of a C–O WD (the He WD case is shown in brackets). The velocity of the wind is $2\eta_{\rm w}^{1/2}$ times the local escape speed, such that the inner disc produces the highest velocity outflow. On larger scales the ejecta forms a singular homologous outflow with a much lower velocity dispersion (see text). At radii $r < R_{\rm in} \sim 10^6$–10^7 cm the temperature is sufficiently high so that nuclei are photodissintegrated into ^{4}He and, ultimately, free neutrons and protons. Near the surface of the NS or BH, cooling by neutrinos may be important if the accretion rate is sufficiently high.

The composition at the outer boundary $r = R_{\rm d}$ is that of the tidally disrupted WD. For C–O WDs we adopt an initial composition $X_{12} = 0.5$ and $X_{16} = 0.5$ (Salaris et al. 1997). We also perform calculations for O–Ne WDs ($X_{16} = 0.7$; $X_{20} = 0.3$; e.g. Gutiérrez, Canal & García-Berro 2005), hybrid He–C–O WDs ($X_4 = 0.2$; $X_{12} = 0.4$; $X_{16} = 0.4$; Han, Tout & Eggleton 2000), and pure He WDs ($X_4 = 1$), although the latter may occur less frequently in Nature due to the limited parameter space available for unstable mass transfer (Section 2). Although we focus on WD–NS binaries, we also consider $3\,{\rm M}_\odot$ BH companions. Table 1 enumerates the models calculated in the next section.

4 RESULTS

Figs 2–5 and Tables 1 and 2 summarize the results of our calculations. In this section we describe the disc structure (Section 4.1), outflow composition (Section 4.2) and thermal stability of our solutions (Section 4.3). In Section 4.4 we discuss the possible effects of convection on our results and in Section 4.5 we present an analytic estimate of the importance of nuclear burning.

4.1 Disc structure

Fig. 2 shows our baseline model for accretion following the merger of a $0.6\,{\rm M}_\odot$ C–O WD with a $1.4\,{\rm M}_\odot$ NS. In this example we adopt characteristic values for the initial accretion rate $\dot{M}(R_{\rm d}) = 3 \times 10^{-3}\,{\rm M}_\odot\,{\rm s}^{-1}$, viscosity $\alpha = 0.1$, disc Bernoulli parameter ${\rm Be}'_{\rm d} = -0.1$ (equation 13) and wind strength $\eta_{\rm w} = 2$. The top panel shows the radial profiles of quantities characterizing the disc thermodynamics. Note the following: (1) the disc is geometrically thick, with aspect ratio $H/r \approx 0.4$ at all radii, as expected for RIAFs; (2) gas pressure $P_{\rm gas}$ exceeds radiation pressure $P_{\rm rad}$, although they are comparable at small radii $\lesssim 10^7$ cm; (3) $\dot{M}$ decreases by a factor of $\sim$10 between $R_{\rm d} \approx 10^9$ cm and the inner radius $R_{\rm in} \approx 10^7$ cm, such that $\gtrsim$80 per cent of the accreting mass escapes in outflows. This behaviour is reflected in the wind mass-loss index p (equation 6), which fluctuates with radius, depending on the local heating/cooling from nuclear reactions.

Table 1. Properties of disc models.

Model	M^a ($\rm M_\odot$)	$M_{\rm WD}$ ($\rm M_\odot$)	$R_{\rm d}{}^b$ (cm)	$\dot{M}(R_{\rm d})$ ($\rm M_\odot\,s^{-1}$)	α	${\rm Be}'_{\rm d}{}^c$	$\eta_{\rm w}{}^d$	$X_A(R_{\rm d})^e$	$\frac{\dot{M}_{\rm wind}}{\dot{M}(R_{\rm d})}{}^f$	$\bar{v}_{\rm ej}{}^g$ ($10^4\,{\rm km\,s^{-1}}$)	Unstable?^{h}
NS_C-O_1	1.4	0.6	10^9	3×10^{-3}	0.1	−0.1	2	$X_{12} = 0.5, X_{16} = 0.5$	0.84	2.8	No
NS_C-O_2	1.4	0.6	10^9	3×10^{-4}	0.01	−0.1	2	–	0.86	2.8	No
NS_C-O_3	1.4	0.6	10^9	3×10^{-3}	0.1	−0.2	1	–	0.99	1.6	No
NS_C-O_4	1.4	0.6	10^9	3×10^{-3}	0.1	0.0	3	–	0.57	3.2	No
NS_C-O-He_1	1.4	0.4	2×10^9	10^{-3}	0.1	−0.1	2	$X_{16} = 0.4, X_{12} = 0.4, X_4 = 0.2$	0.95	2.5	Yes
NS_C-O-He_2	1.4	0.4	2×10^9	10^{-4}	0.01	−0.1	2	–	0.95	2.4	Yes
NS_O-Ne^i	1.4	1.2	2×10^8	10^{-1}	0.1	–	–	$X_{16} = 0.6, X_{20} = 0.4$	–	–	Yes
BH_C-O_1	3	1.0	5×10^8	3×10^{-2}	0.1	−0.2	2	$X_{12} = 0.5, X_{16} = 0.5$	0.72	3.6	Yes
BH_C-O_2	3	1.0	5×10^8	3×10^{-3}	0.01	−0.2	2	–	0.72	3.6	Yes
BH_C-O_3	3	1.0	5×10^8	3×10^{-2}	0.1	−0.25	1	–	0.96	2.3	Yes
BH_O-Ne_1	3	1.2	5×10^8	3×10^{-2}	0.1	−0.2	2	$X_{16} = 0.6, X_{20} = 0.4$	0.83	4.6	Yes
BH_O-Ne_2	3	1.2	5×10^8	3×10^{-3}	0.01	−0.2	2	–	0.72	3.5	Yes
NS_He_1	1.2	0.3	2×10^9	10^{-3}	0.1	−0.1	2	$X_4 = 1$	0.95	2.2	No
NS_He_2	1.2	0.3	2×10^9	10^{-4}	0.01	−0.1	2	–	0.96	2.0	No
NS_He_3	1.2	0.3	2×10^9	10^{-3}	0.1	−0.2	1	–	0.99	1.0	No

^{a}Mass of the central NS or BH. ^{b}Outer edge of the disc $R_{\rm d} = R_{\rm RLOF}(1+q)^{-3}$, where $q \equiv M_{\rm WD}/M$ and $R_{\rm RLOF}$ is the binary separation at RLOF (equation 2). ^{c}Normalized Bernoulli parameter in the disc (equation 13). ^{d}Ratio of the specific kinetic energy of the wind from any radius to the local gravitational binding energy. ^{e}Initial composition of the disc from the disrupted WD. ^{f}Ratio of the total mass-loss rate in the wind $\dot{M}_{\rm w} \equiv \dot{M}(R_{\rm d}) - \dot{M}(R_{\rm in})$ to the initial accretion rate $\dot{M}(R_{\rm d})$ at the outer edge of the disc. ^{g}Mean velocity of the ejecta from disc winds (equation 18). ^{h}Whether the disc is thermally unstable due to nuclear burning at any radius, according to the most stringent criterion $f_{\rm nuc} < f_{\rm nuc,th2}$ given in equation (20). ^{i}Characteristic values shown for illustration only. The disc model presented in this paper cannot be applied to the merger of massive WD–NS binaries because nuclear burning begins already at $r \approx R_{\rm d}$ (see Section 4.2).

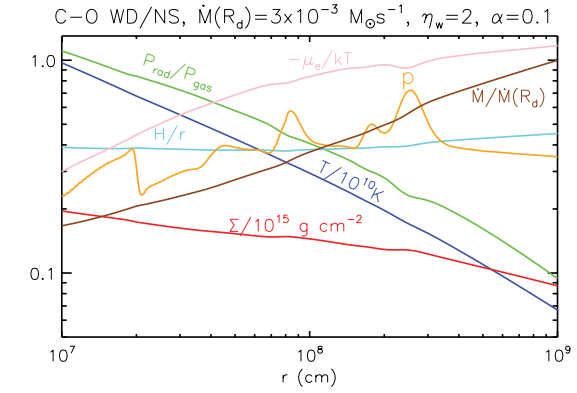

(a) Radial Profile of Disk Properties

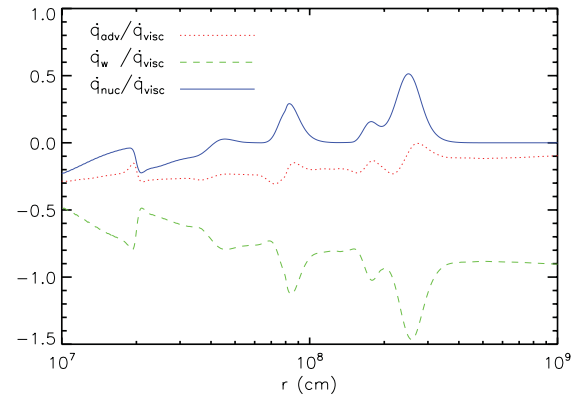

(b) Heating/Cooling Terms in the Entropy Equation

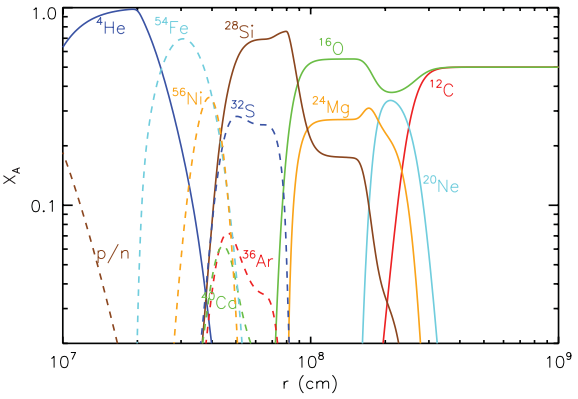

(c) Composition Profile

Figure 2. Accretion following the merger of a 0.6 $M_\odot$ WD with a 1.4 $M_\odot$ NS. We adopt fiducial values $\eta_w = 2$ for the wind efficiency, $Be'_d = -0.1$ for the Bernoulli function of the disc (equation 13) and $\alpha = 0.1$ for the disc viscosity. The latter translates into an accretion rate $\dot{M}(R_d) \simeq 3\times10^{-3}\,M_\odot\,s^{-1}$ at the outer edge of the disc $R_d = 10^9$ cm (equation 4). Top: disc temperature T (blue), surface density Σ (red), aspect ratio H/r (turquoise), ratio of radiation to gas pressure P_{rad}/P_{gas} (green), negative of the electron chemical potential μ_e divided by kT (pink), accretion rate $\dot{M}$ normalized to $\dot{M}(R_d)$ (brown) and wind mass-loss index p (orange; equation 6) as a function of radius. Middle: contributions of various sources of heating and cooling divided by the viscous heating rate $\dot{q}_{visc}$: nuclear reactions $\dot{q}_{nuc}$ (solid blue); advective cooling within the disc $\dot{q}_{adv} \equiv T v_r(\partial s/\partial r)$ (solid dotted); and wind cooling $\dot{q}_w$ (dashed green; equation 14). Bottom: mass fraction X_A of various isotopes in the disc mid-plane.

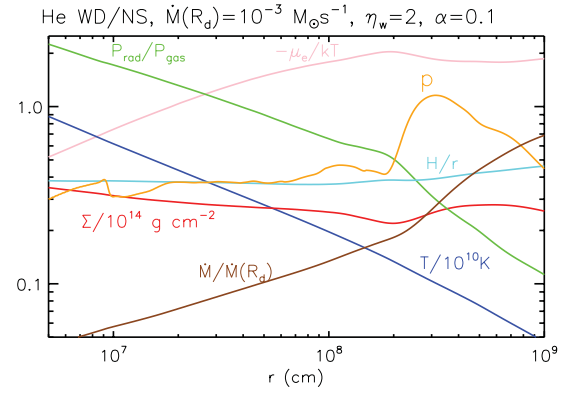

(a) Radial Profile of Disk Properties

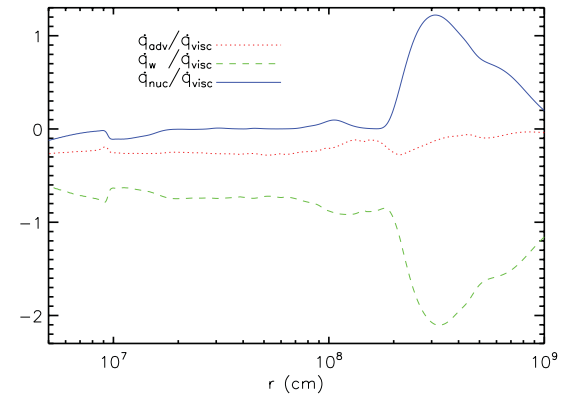

(b) Heating/Cooling Terms in the Entropy Equation

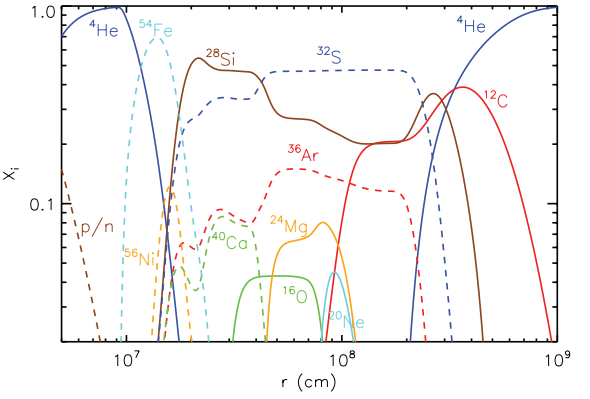

(c) Composition Profile

Figure 3. Similar to Fig. 2, but calculated for a pure He WD. Values of $\eta_w = 2$, $Be'_d = -0.1$ and $\alpha = 0.1$ are the same as the C–O case, but the latter corresponds to a lower accretion rate $\dot{M}(R_d) \simeq 10^{-3}\,M_\odot\,s^{-1}$ due to the larger outer radius $R_d = 2\times10^9$ cm.

The middle panel in Fig. 2 shows sources of heating and cooling that contribute to the entropy equation (equation 11), in ratio to the viscous heating rate $\dot{q}_{visc}$ (equation 12). At large radii ($r \gtrsim 5\times10^7$ cm), both viscous dissipation and nuclear burning contribute to the heating, while cooling results from advection to smaller radii $\dot{q}_{adv}$ and mass-loss due to winds $\dot{q}_w$ (equation 14). The nuclear heating rate achieves local maxima at radii where the temperature reaches the threshold necessary to burn the next element (e.g. carbon burns at $r \approx 3\times10^8$ cm and $T \approx 1.5\times10^9$ K). At these locations

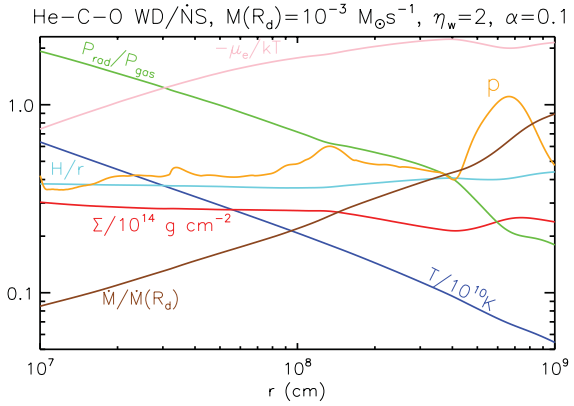

(a) Radial Profile of Disk Properties

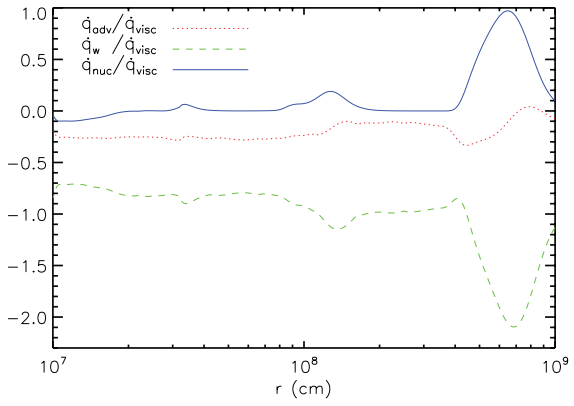

(b) Heating/Cooling Terms in the Entropy Equation

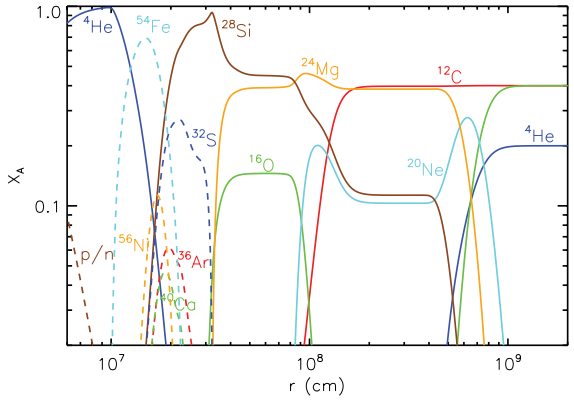

(c) Composition Profile

Figure 4. Same as Fig. 3, but calculated for a 'hybrid' He–C–O WD.

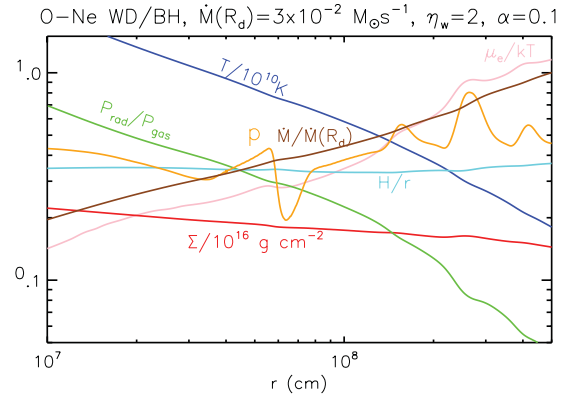

(a) Radial Profile of Disk Properties

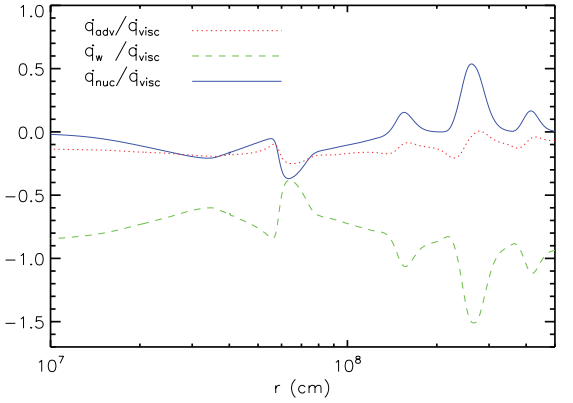

(b) Heating/Cooling Terms in the Entropy Equation

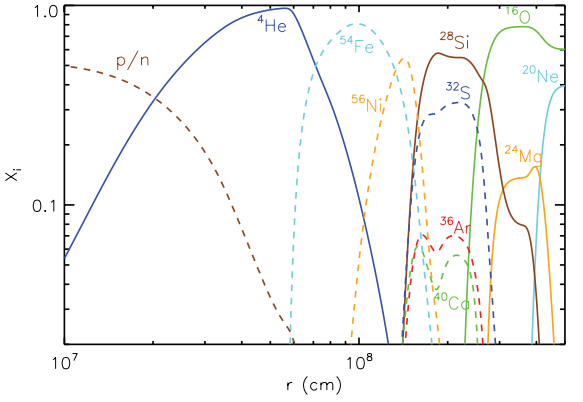

(c) Composition Profile

Figure 5. Similar to Figs 2–4, but calculated for the merger of a O–Ne WD with a $3\,M_\odot$ BH. We adopt values of $\eta_w = 2$, $Be'_d = -0.2$, $\alpha = 0.1$, $\dot{M}(R_d) \simeq 3 \times 10^{-3}\,M_\odot\,s^{-1}$ and $R_d = 5 \times 10^8$ cm.

the energy generated by nuclear reactions is significant compared to that released by viscous dissipation; this general behaviour has important implications for the thermal stability of the disc (Section 4.3). At smaller radii ($r \lesssim 5 \times 10^7$ cm), by contrast, $\dot{q}_{\rm nuc} < 0$ instead contributes to *cooling* the disc. This occurs once temperatures are sufficiently high ($T \gtrsim 6 \times 10^9$ K) to photodisintegrate nuclei *endothermically*.

The bottom panel of Fig. 2 shows the mass fractions of individual elements X_A as a function of radius. The composition at the outer edge of the disc is that of the initial WD: half ^{12}C and half ^{16}O. Moving to smaller radii, carbon first burns to ^{20}Ne and ^{4}He, the latter of which rapidly captures on to ^{16}O, eventually forming ^{24}Mg. At smaller radii and higher temperatures, ^{16}O burns to ^{28}Si. Moving yet further in, photodissociation releases α particles, which immediately capture on to heavier nuclei ('Si burning'), producing ^{32}S, ^{36}Ar, ^{40}Ca, ^{56}Ni and ^{54}Fe. Finally, at the smallest radii, ^{54}Fe photodisintegrates into ^{4}He, which itself then disintegrates into free protons and neutrons.

In Fig. 3 we show similar results to Fig. 2, but for the case of a $0.3\,M_\odot$ pure He WD. We adopt the same values for $\eta_w = 2$, $Be'_d = -0.1$ and $\alpha = 0.1$, but the latter corresponds to a lower accretion rate $\dot{M}(R_d) \simeq 10^{-3}\,M_\odot\,s^{-1}$ than in the C–O WD case,

Table 2. Elemental mass fractions in the wind ejecta $X_{w,A}$ (equation 17).

Model	^{4}He	^{12}C	^{16}O	^{20}Ne	^{24}Mg	^{28}Si	^{32}S	^{36}Ar	^{40}Ca	^{44}Ti	^{48}Cr	^{52}Fe	^{54}Fe	^{56}Ni
W7 Ia[a]	0.0	0.036	0.10	0.0014	0.0094	0.11	0.060	0.11	0.0086	5.7×10^{-6}	3.5×10^{-9}	–	0.054	0.42
NS_C-O_1	0.063	0.26	0.39	0.049	0.065	0.10	0.023	0.0043	0.0031	2.1×10^{-5}	1.0×10^{-4}	9.7×10^{-4}	0.032	0.011
NS_C-O_2	0.052	0.26	0.38	0.058	0.067	0.096	0.021	0.0036	0.0025	1.3×10^{-5}	7.0×10^{-5}	8.0×10^{-4}	0.042	0.011
NS_C-O_3	0.0091	0.41	0.47	0.029	0.034	0.034	0.0068	0.0012	8.0×10^{-4}	3.7×10^{-6}	1.4×10^{-5}	1.0×10^{-4}	0.0061	1.0×10^{-3}
NS_C-O_4	0.070	0.21	0.36	0.057	0.076	0.13	0.029	0.0055	0.0040	2.6×10^{-5}	1.3×10^{-4}	0.0012	0.035	0.014
NS_C-O-He_1	0.12	0.33	0.18	0.093	0.16	0.087	0.0064	0.0010	6.5×10^{-4}	4.2×10^{-6}	1.6×10^{-5}	1.2×10^{-4}	0.010	0.0010
NS_C-O-He_2	0.11	0.33	0.17	0.095	0.19	0.071	0.0054	9.5×10^{-4}	7.1×10^{-4}	4.5×10^{-6}	2.3×10^{-5}	2.3×10^{-4}	0.011	0.0027
BH_C-O_1	0.15	6.7×10^{-4}	0.20	0.043	0.11	0.24	0.047	0.0081	0.0063	4.8×10^{-5}	2.9×10^{-4}	0.0036	0.12	0.053
BH_C-O_2	0.14	5.7×10^{-5}	0.19	0.021	0.098	0.25	0.047	0.0062	0.0039	1.2×10^{-5}	6.3×10^{-5}	7.4×10^{-4}	0.22	0.011
BH_C-O_3	0.062	0.12	0.30	0.10	0.098	0.17	0.032	0.0053	0.0040	3.0×10^{-5}	1.8×10^{-4}	0.0021	0.065	0.031
BH_O-Ne_1	0.15	4.7×10^{-6}	0.30	0.045	0.035	0.17	0.076	0.016	0.013	5.5×10^{-5}	3.0×10^{-4}	0.0036	0.12	0.054
BH_O-Ne_2	0.13	2.8×10^{-6}	0.27	0.024	0.037	0.18	0.080	0.015	0.011	1.8×10^{-5}	6.6×10^{-5}	7.1×10^{-4}	0.22	0.010
Shen10.Ia[b]	0.30–0.45	–	–	–	–	–	–	$6–700 \times 10^{-5}$	0.001–0.04	0.007 – 0.1	0.01 – 0.1	0.03 – 0.1	–	0.1-0.7
NS_He_1	0.63	0.15	0.0022	0.0017	0.0055	0.095	0.082	0.018	0.0027	7.1×10^{-6}	1.8×10^{-5}	1.1×10^{-4}	0.0082	9.7×10^{-4}
NS_He_2	0.60	0.23	0.0031	0.0036	0.016	0.13	0.013	7.8×10^{-4}	4.3×10^{-4}	2.7×10^{-6}	1.4×10^{-5}	1.4×10^{-4}	0.0068	1.6×10^{-3}
NS_He_3	0.87	0.077	4.3×10^{-4}	4.7×10^{-4}	0.0014	0.024	0.024	0.0092	7.7×10^{-4}	1.4×10^{-6}	1.0×10^{-6}	1.8×10^{-6}	4.0×10^{-4}	5.3×10^{-6}

[a]W7 SN Ia model (Nomoto et al. 1984); [b]range of models for unstable He shell burning from Shen et al. (2010).

due to the larger outer radius $R_{\rm d} = 2 \times 10^{9}$ cm. The qualitative disc structure is similar to the C–O case, but a few differences should be noted. First, mass-loss is considerably greater from the outer portions of the disc ($p \gtrsim 1$). This is due to the substantial energy released by He burning and its low threshold temperature; burning thus occurs at large radii where the gravitational potential is shallow. Mass-loss greatly reduces the mid-plane density, which increases the importance of radiation pressure. Because the temperature is lower in radiation-dominated discs than in gas pressure-dominated discs, burning heavier elements is delayed until smaller radii than in the C–O case. Also note that the production of ^{16}O, ^{20}Ne and ^{24}Mg are largely bypassed (e.g. in comparison to the C–O case) because additional α captures are rapid following the onset of the (rate-limiting) triple-α reaction.

Fig. 4 shows results for a $0.4\,{\rm M}_{\odot}$ 'hybrid' He–C–O WD, again for an accretion rate $\dot{M}(R_{\rm d}) = 10^{-3}\,{\rm M}_{\odot}\,{\rm s}^{-1}$. Although the inner structure of the disc resembles the C–O case (Fig. 2), an important difference is again the onset of He burning at relatively large radii (low temperature), this time via the reaction $^{4}{\rm He} + {}^{16}{\rm O} \rightarrow {}^{20}{\rm Ne} + \gamma$. As we discuss in Section 4.3, the sensitive temperature dependence of this reaction may render such discs thermally unstable.

Fig. 5 shows results for a $1.2\,{\rm M}_{\odot}$ O–Ne WD accreting on to a $3\,{\rm M}_{\odot}$ BH. The compact outer radius of the disc in this case $R_{\rm d} \simeq 5 \times 10^{8}$ cm results in a high accretion rate $\dot{M}(R_{\rm d}) \simeq 3 \times 10^{-2}\,{\rm M}_{\odot}\,{\rm s}^{-1}$ for $\alpha = 0.1$. Without He or C present, the first element to burn in this case is ^{20}Ne at $T \approx 2 \times 10^{9}$ K, but otherwise the composition profile is similar to the C–O case (Fig. 2).

In addition to the calculations presented above, we have explored the sensitivity of our results to variations in the binary parameters, WD composition, viscosity α and wind mass-loss parameter $\eta_{\rm w}$ (see Table 2). In general, we find that increasing $\eta_{\rm w}$ at fixed $\mathrm{Be}'_{\rm d}$ decreases the amount of mass-loss because wind cooling is more effective. By contrast, changing α [along with a compensating change in $\dot{M}(R_{\rm d})$; equation 4] has a smaller effect. Our results are also robust to realistic variations in the composition of the disrupted WD.

Notably absent from the discussion thus far is the merger of a massive C–O or O–Ne WD with a NS companion. The large mass ratio $q \sim 1$ in this case results in a compact disc ($R_{\rm d} \sim 10^{8}$ cm) with a very high initial accretion rate $\dot{M}(R_{\rm d}) \approx 0.1\,{\rm M}_{\odot}\,{\rm s}^{-1}$ for $\alpha = 0.1$. The initial temperature of the disc is sufficiently high so that nuclear burning begins already at $r \approx R_{\rm d}$ during the circularization process itself. Since virialization has not yet occurred, the WD material forming the disc may still be degenerate, potentially leading to an explosive situation. Furthermore, as we discuss in Section 4.3, accretion in these systems may be thermally unstable, even under non-degenerate conditions. Clearly, many of the simplifications adopted in our model break down in the case of massive WD–NS mergers. Obtaining even a qualitative understanding of such events may require multidimensional simulations that include the effects of nuclear burning, even during the merger process itself.

4.2 Outflow properties

A schematic diagram of the outflows from WD–NS/BH merger discs is shown in Fig. 1. The total mass-loss rate from the disc is approximately given by $\dot{M}_{\rm w} \simeq \dot{M}(R_{\rm d}) - \dot{M}(R_{\rm in})$, where $R_{\rm in} \sim 10^{6.5}$–$10^{7.5}$ cm is the radius interior to which the disc is primarily free nucleons. We adopt this inner boundary because if neutrino cooling is important at radii $r < R_{\rm in}$, then additional mass-loss will be suppressed (although in Section 5.2 we discuss the possibility that the ejecta does contain a small fraction of free nucleons). If most of the WD accretes at the characteristic rate $\dot{M}(R_{\rm d})$ (equation 4),

then the total ejecta mass is $M_{\rm ej} \approx f_{\rm ej} M_{\rm WD}$, where $f_{\rm ej} = \left[\frac{\dot{M}_{\rm w}}{\dot{M}_{\rm d}(R_{\rm d})}\right]$ is the fraction of the accreted mass lost in winds. Depending on $\eta_{\rm w}$, we find that $f_{\rm w} \sim 0.5$–0.99[0.90–0.99] for C–O[He] WDs (Table 2), corresponding to $M_{\rm ej} \sim 0.3$–1.3[0.3] $\rm M_\odot$.

The radial structure of the disc is imprinted on the composition of the outflows (Fig. 1). Table 2 provides the mass fractions in each element of the wind ejecta, which are calculated as

$$X_{{\rm w},A} = \frac{1}{\dot{M}_{\rm w}} \int_{R_{\rm in}}^{R_{\rm d}} X_A \frac{\partial \dot{M}_{\rm w}}{\partial r}\, {\rm d}r. \quad (17)$$

Here we have assumed that the local surface composition of the disc is similar to that in the mid-plane due e.g. to turbulent mixing. To compare with our C–O disc models, we also list the abundances predicted by the well-studied 'W7' model for SN Ia from the delayed detonation of a Chandrasekhar-mass C–O WD (Nomoto et al. 1984). To compare with our He disc models, we list the range in ejecta abundances predicted from models for unstable He shell burning on the surface of a C–O WD, as calculated by Shen et al. (2010) for different values of the mass of the WD and He layer.

In our fiducial C/O model (Fig. 2) the majority of the ejecta is unburnt ^{12}C (26 per cent) and ^{16}O (39 per cent), with the remainder in ^{28}Si (10 per cent), ^{24}Mg (7 per cent), ^{4}He (6 per cent), ^{20}Ne (5 per cent), ^{54}Fe (3 per cent), ^{32}S(2 per cent), ^{56}Ni (1.1 per cent), ^{36}Ar (0.4 per cent) and ^{40}Ca (0.3 per cent). Compared to the W7 SN Ia model, the fractional abundances of unburnt C/O, ^{20}Ne and ^{24}Mg are significantly higher. Despite these differences, the abundances of the elements Si, S and Ca, generally responsible for producing the most prominent spectral features in normal SN Ia, are similar to the W7 model within a factor of $\lesssim$ 2–3. Importantly, the yield of radioactive ^{56}Ni is substantially lower than in normal SN Ia ejecta; this has important implications for the luminosities of optical transients associated with WD–NS/BH mergers (Section 5.2).

In our fiducial He model (Fig. 3) the vast majority of the ejecta is unburnt ^{4}He (63 per cent), with the remainder in ^{12}C (15 per cent), ^{28}Si (10 per cent), ^{32}S(8 per cent), ^{36}Ar (2 per cent), ^{54}Fe (0.8 per cent), ^{24}Mg (0.6 per cent), ^{40}Ca (0.3 per cent), ^{20}Ne (0.2 per cent), ^{16}O (0.2 per cent) and ^{56}Ni (0.1 per cent). Although the unburnt ^{4}He fraction is similar to the He shell burning models of Shen et al. (2010), the predicted abundances of the radioactive isotopes ^{44}Ti, ^{48}Cr and ^{56}Ni are all significantly lower, while those of intermediate-mass elements are significantly higher. In addition to the above elements, disc outflows may in all cases also contain a tiny fraction of ^{1}H from the very inner disc, the implications of which are briefly discussed in Section 5.2.

Winds from smaller radii in the disc achieve higher velocities $v_{\rm w} \propto v_{\rm k} \propto r^{-1/2}$ than those from further out. Nevertheless, most of the ejecta will ultimately reside in a single 'shell' of material with a much lower velocity dispersion. This is because, initially after the disruption (on time-scales $t \ll t_{\rm visc}$; equation 3), the disc is concentrated at large radii $\approx R_{\rm d}$. Slow outflows from this early stage will thus have time to encase the system before outflows have even begun in earnest from the inner disc on a time-scale $t \gtrsim t_{\rm visc}$. Fast ejecta from the inner disc will thus collide with the slower material ejected prior. Because this interaction conserves energy (radiative losses are negligible at early times), the ejecta will achieve a mean velocity $\bar{v}_{\rm ej}$, which may be estimated by averaging over the total kinetic energy of winds from each disc annulus:

$$\frac{1}{2} M_{\rm ej} \bar{v}_{\rm ej}^2 = \frac{1}{2} \int_{R_{\rm in}}^{R_{\rm d}} \frac{\partial \dot{M}_{\rm w}}{\partial r} v_{\rm w}^2\, {\rm d}r. \quad (18)$$

Table 2 shows that for C–O WD/NS mergers $\bar{v}_{\rm w}$ is typically $\sim$1–$3 \times 10^4\,{\rm km\,s^{-1}}$, while for He[O–Ne] mergers $v_{\rm w}$ is somewhat lower[higher].

The reason that $\bar{v}_{\rm w}$ can exceed the typical velocity of SN Ia ejecta is the deeper gravitational potential well in the case of NS/BH accretion. As a toy example, if mass-loss were to occur with a constant power-law index $p = {\rm const} < 1$ (equation 6), then integrating equation (18) gives

$$\bar{v}_{\rm ej} \simeq \begin{cases} \left[\dfrac{p\eta_{\rm w}}{1-p}\dfrac{GM}{R_{\rm in}}\left(\dfrac{R_{\rm in}}{R_{\rm d}}\right)^{p}\right]^{1/2}, & p < 1 \\ \left[\eta_{\rm w}\dfrac{GM}{R_{\rm d}}\ln\left(\dfrac{R_{\rm d}}{R_{\rm in}}\right)\right]^{1/2}, & p = 1 \end{cases}, \quad (19)$$

where in the first expression we have assumed that $R_{\rm d} \gg R_{\rm in}$. A larger wind efficiency factor $\eta_{\rm w}$ thus increases $\bar{v}_{\rm ej}$, both because $v_{\rm w} \propto \eta_{\rm w}^{1/2}$ and because larger $\eta_{\rm w}$ decreases the mass-loss rate $p(r)$ required to cool the disc. Equation (19) shows that (for $\eta_{\rm w} \simeq 1$) the minimum value of $v_{\rm ej}$ ($p \approx 1$) is of the order of the orbital velocity at $r \approx R_{\rm d}$. This varies from $\approx 3 \times 10^3\,{\rm km\,s^{-1}}$ for He WD–NS mergers to $\approx 10^4\,{\rm km\,s^{-1}}$ for O–Ne WD–NS/BH mergers.

4.3 Thermal stability

The calculations presented in the previous sections assumed steady-state accretion. This is not valid, however, if the disc is thermally unstable, which might be expected due to the sensitive temperature dependencies of nuclear reactions. The criterion for thermal stability may be written (Piran 1978) as

$$\left.\frac{\partial \ln q^+}{\partial \ln H}\right|_\Sigma < \left.\frac{\partial \ln q^-}{\partial \ln H}\right|_\Sigma \rightarrow \left.\frac{\partial \ln q^+}{\partial \ln P}\right|_\Sigma < \left.\frac{\partial \ln q^-}{\partial \ln P}\right|_\Sigma, \quad (20)$$

where $q^+ = \dot{q}_{\rm visc} + \dot{q}_{\rm nuc}$ and $\dot{q}^- = \dot{q}_{\rm adv} + \dot{q}_{\rm w}$ are the total heating and cooling rates, respectively (see equation 11), and the second condition follows because $P = \rho a^2 \propto \Omega_{\rm k}^2 \Sigma H$. Viscous heating obeys $\dot{q}_{\rm visc} \propto P^2$, while advective cooling obeys $\dot{q}_{\rm adv} \propto \dot{q}_{\rm visc}(H/r)^2 \propto P^4$. In our model, we have assumed that the terminal speed of disc winds $v_{\rm w}$ is proportional to the local escape speed $\propto v_{\rm k}$ (equation 14), such that $\dot{q}_{\rm w} \propto \dot{q}_{\rm visc} \propto P^2$. However, the precise mechanism responsible for driving the wind is uncertain; we could equally well have assumed that $v_{\rm w}$ is proportional to the sound speed a, in which case $\dot{q}_{\rm w} \propto (H/r)^2 v_{\rm k} \propto P^4$. Considering both cases, the stability criterion in equation (20) can equivalently be written as an upper limit on the fraction $f_{\rm nuc} \equiv \dot{q}_{\rm nuc}/\dot{q}^+$ of the disc heating supplied by nuclear reactions, viz.

$$f_{\rm nuc} < \begin{cases} \dfrac{2(1-f_{\rm w})}{n-2} \equiv f_{\rm nuc,th1}, & v_{\rm w} \propto v_{\rm esc}, \\ \dfrac{2}{n-2} \equiv f_{\rm nuc,th2}, & v_{\rm w} \propto a, \end{cases} \quad (21)$$

where $n \equiv \left(\frac{\partial \ln \dot{q}_{\rm nuc}}{\partial \ln P}\right)|_\Sigma$ and $f_{\rm w} \equiv \dot{q}_{\rm w}/\dot{q}^-$ is the fraction of the cooling resulting from winds. Equation (21) shows that accretion is stable at a given radius if either (1) nuclear burning is absent entirely or (2) the burning rate has a weak pressure dependence $n < 4 - 2f_{\rm w}$ or $n < 4$, in the cases $v_{\rm w} \propto v_{\rm k}$ and $v_{\rm w} \propto a$, respectively.

Fig. 6 shows $f_{\rm nuc}$ (solid line), $f_{\rm nuc,th1}$ (solid lines) and $f_{\rm nuc,th2}$ as a function of radius, calculated for our solution from Section 4 corresponding to accretion following a $0.6\,\rm M_\odot$ C–O WD (Fig. 2). Fig. 6 shows that in the case $v_{\rm w} \propto a$, the disc is stable at all radii, i.e. $f_{\rm nuc} < f_{\rm nuc,th2}$. If, however, we instead assume that $v_{\rm w} \propto v_{\rm k}$, then we find that the disc is unstable ($f_{\rm nuc} > f_{\rm th1}$) at the radii $\sim$ few $\times 10^8$ cm where carbon burning peaks. Although we do not show this case

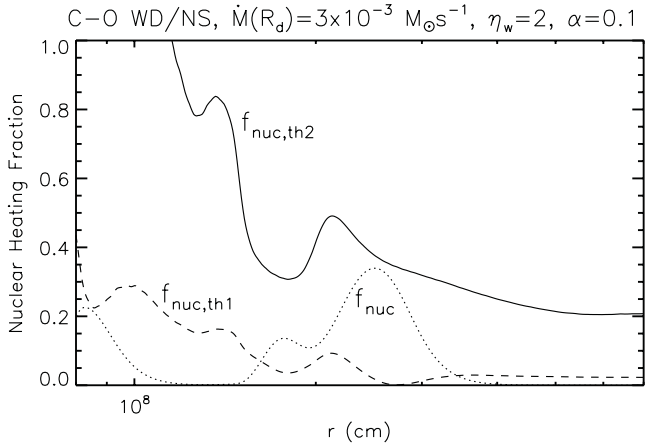

(a) $0.6M_\odot$ WD/NS

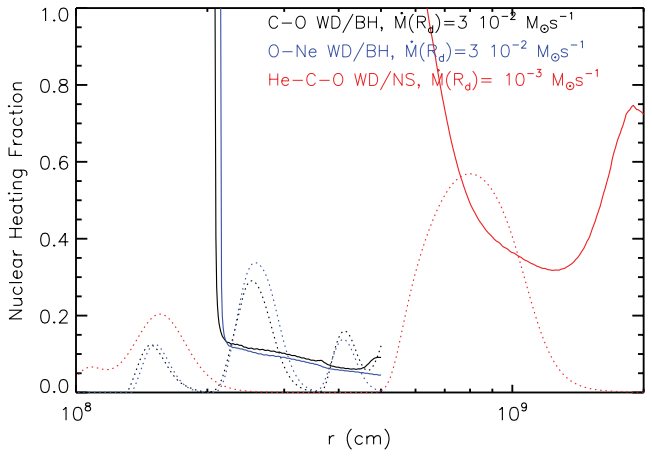

(b) $0.4M_\odot$ He-C-O/NS, $1.0M_\odot$ WD/BH, and $1.2M_\odot$ WD/BH

Figure 6. Analysis of the thermal stability of the accretion solutions presented in Section 4.1. Quantities shown are the fraction of the total heating due to nuclear burning $f_{\rm nuc} \equiv \dot{q}_{\rm nuc}/\dot{q}^+$ (dotted line) and the threshold fractions for thermal instability $f_{\rm nuc,th1}$ (dashed line) and $f_{\rm nuc,th2}$ (solid line) under the assumption that $v_{\rm w} \propto v_k$ and $v_{\rm w} \propto a$, respectively (equation 21). Top: solutions corresponding to accretion following the merger of a $0.6\,{\rm M}_\odot$ $1.4\,{\rm M}_\odot$ WD with a NS at the rate $\dot{M}(R_{\rm d}) = 3 \times 10^{-3}\,{\rm M}_\odot\,{\rm s}^{-1}$ (Fig. 2). Note that although $f_{\rm nuc} < f_{\rm nuc,th2}$ at all radii, $f_{\rm nuc}$ exceeds $f_{\rm nuc,th1}$ across some range in radius. This shows that whether the disc is in fact stable depends on the detailed pressure dependence of wind cooling. Bottom: accretion following the merger of a $1\,{\rm M}_\odot$ C–O WD with a $3\,{\rm M}_\odot$ BH (black); $1.2\,{\rm M}_\odot$ O–Ne WD with a $3\,{\rm M}_\odot$ BH (blue); 'hybrid' He–C–O WD with a $1.4\,{\rm M}_\odot$ NS (red). In all three cases $f_{\rm nuc} > f_{\rm nuc,th2}$ over some range in radii. The solutions are thus unstable to runaway heating from nuclear burning, regardless of whether $v_{\rm w} \propto v_k$ or $v_{\rm w} \propto a$.

explicitly, we find a similar result for He WDs: the triple-α reaction is not sufficiently pressure sensitive for instability if $v_{\rm w} \propto a$ (i.e. $n < 4$), but for $v_{\rm w} \propto v_{\rm k}$ the disc is unstable at radii $\sim$3–4 $\times\ 10^8$ cm where He burning peaks. We conclude that whether C–O or He WD discs are thermally stable depends on the pressure dependence of wind cooling, which in turn depends on the (uncertain) mechanism responsible for driving the wind.

In the case of O–Ne and hybrid WDs, thermal instability seems more assured. In the bottom panel of Fig. 6 we show $f_{\rm nuc}$ and $f_{\rm nuc,th2}$ (equation 21) for cases corresponding to the merger of a $0.4\,{\rm M}_\odot$ He–C–O WD with a NS (Fig. 4); a $1.2\,{\rm M}_\odot$ O–Ne WD with a $3\,{\rm M}_\odot$ BH (Fig. 5) and a $1.0\,{\rm M}_\odot$ C–O WD with a $3\,{\rm M}_\odot$ BH. In all three cases we find that over some range of radii, $f_{\rm nuc}$ exceeds even the more conservative threshold for instability $f_{\rm nuc,th2}$. This implies that our calculated solutions are thermally unstable, independent of whether $v_{\rm w} \propto v_{\rm k}$ or $v_{\rm w} \propto a$. Although addressing the implications of unstable burning is beyond the scope of this paper, we speculate that the end result may be a complicated, time-dependent evolution. One possibility is 'limit-cycle' behaviour, in which the initial inflow is halted by runaway burning, before resuming again later with fresh fuel (a possible analogue are dwarf nova outbursts of cataclysmic variables; e.g. Cannizzo 1993). Though it is not obvious, the steady-state solutions constructed here may remain a reasonable description of the average flow over many cycles.

4.4 Effects of convection

It is well known that ADAFs are unstable to radial convection (Narayan & Yi 1994; Igumenshchev, Abramowicz & Narayan 2000; Quataert & Gruzinov 2000). In the case of NuDAFs, the disc may also be unstable to *vertical* convection because the nuclear heating peaks sharply near the mid-plane due to its sensitive temperature dependence. Although our calculations have thus far neglected its effects on the transport of angular momentum, energy and composition, in this section we describe how strong convection could alter our conclusions.

If convection transports angular momentum outwards – similar to MHD turbulence produced by the MRI – then it would act simply to enhance the effective value of 'α', which we have shown does not qualitatively affect our results. If, on the other hand, convection transports angular momentum inwards (Ryu & Goodman 1992), then a qualitatively different type of solution could be obtained: a 'convection-dominated accretion flow' (CDAF; Narayan, Igumenshchev & Abramowicz 2000; Quataert & Gruzinov 2000). In CDAFs, the angular momentum transported outwards by viscosity is balanced by the inward transport by convection, such that the net mass accretion rate is very small. Because in steady state the convective energy flux $F_{\rm c} \propto \rho c_{\rm s}^3 r^2$ is constant with radius, CDAFs are characterized by a more shallow density profile $\rho \propto r^{-1/2}$ than for normal ADAF solutions ($\rho \propto r^{-3/2}$). If present, the CDAF would extend from the inner edge of the RIAF at $R_{\rm in} \sim 10^6$–10^7 cm to much larger radii, where the outflowing energy is released through radiation or outflows.

Coincidentally, the density profile of a CDAF scales the same way with radius as in ADIOS (wind) models with 'maximal' mass-loss ($p = 1$; $\dot{M} \propto r$). Our steady-state calculations with high mass-loss rates (low $\eta_{\rm w}$) thus may also be applied to the CDAF case. Note, however, that the physical interpretation is completely different: in wind models, the outflowing mass escapes the system entirely, while in CDAFs it remains bound and is simply 'recycled' by mixing to large radii, from which it accretes again later.

If the outer edge of the disc remains near the initial radius of the disrupted WD $R_{\rm d}$, then convection simply increases the timescale for matter to accrete from that given in equation (3) by a factor $\sim \frac{\dot{M}(R_{\rm d})}{\dot{M}(R_{\rm in})} \sim \frac{R_{\rm d}}{R_{\rm in}} \sim 10$–$10^3$, or from minutes to hours or days. The radial structure of the disc is similar to the maximal wind case, but the observational signature of the event as described in Section 5 will be altered. With no outflows present, the central NS or BH accretes significantly more mass, potentially resulting in more energetic high-energy emission (Section 5.1). On the other hand, with little or no radioactive material ejected, the SN-like optical counterpart (if any) would be much dimmer (Section 5.2). Outflows

may still occur from the outer radius of the CDAF in this scenario, but the mean velocity is likely be much lower and the ^{56}Ni fraction would be smaller.

A more radical possibility is that the outward convective energy flux will 'feed back' on the outer disc, altering its dynamics entirely. If pressure forces cause the outer reservoir of mass to expand significantly from its initial radius $\sim R_{\rm d}$, then rotational support will no longer be important. As a much larger, quasi-spherical accreting envelope, the structure may thus come to resemble a similar 'Thorne–Zytkow object' (Thorne & Zytkow 1975) or 'quasi-star' (e.g. Begelman, Rossi & Armitage 2008). In this case, the accretion time-scale will be even long than estimated above, because it instead depends on the rate that the convective energy escapes the outer boundary in radiation or winds. A quantitative exploration of such a model is an important and interesting exercise for future work, but is beyond the scope of this paper.

Despite the important possible effects of convection discussed above, it is not clear that CDAFs are in fact relevant to WD–NS/BH mergers. As already noted, whether the flow is best described as a CDAF or ADAF (with winds) depends on the strength (and direction) of convective angular momentum transport relative to other torques. Although radial convection in hydrodynamic simulations of RIAFs indeed appears to balance outward viscous transport for $\alpha \lesssim 0.05$ (Narayan et al. 2000, 2002), higher values of $\alpha \sim 0.1$ are generally inferred from observations of ionized discs in a variety of astrophysical contexts (King, Pringle & Livio 2007b). In WD–NS/BH mergers, angular momentum transport due to gravitational instabilities may also compete with convection. Finally, it has been argued that global MHD simulations of RIAFs more closely resemble the ADIOS picture of outflows employed in this paper (Hawley, Balbus & Stone 2001; Hawley & Balbus 2002), although this conclusion may depend on the (uncertain) saturation strength of the MRI and the ultimate fate of the mass leaving the grid.

4.5 Analytic estimate of the importance of nuclear burning

We conclude this section with an analytic estimate of the importance of nuclear burning in hyper-accreting discs, i.e. we address when a disc is in the NuDAF regime. Focusing on the burning of one isotope A, the nuclear heating rate may be written as $\dot{q}_{\rm nuc} = \Delta\epsilon_{\rm nuc}/m_{\rm n}t_{\rm burn}$, where $\Delta\epsilon_{\rm nuc} = X_A Q/A$ is the nuclear energy released per nucleon, Q is the Q-value of the reaction, $m_{\rm n}$ is the nucleon mass, $t_{\rm burn} = \Delta r_{\rm burn}/v_{\rm r}(r_{\rm burn})$ is the time spent burning at radius $r = r_{\rm burn}$, $v_r = 3\nu/2r$ is the accretion velocity and $\Delta r_{\rm burn}$ is the radial distance over which most of the energy is released. The ratio of nuclear to viscous heating can thus be written as

$$\left.\frac{\dot{q}_{\rm nuc}}{\dot{q}_{\rm visc}}\right|_{r=r_{\rm burn}} = \left.\frac{\Delta\epsilon_{\rm nuc}/m_{\rm n}t_{\rm burn}}{(9/4)\nu\Omega_k^2}\right|_{r=r_{\rm burn}} = \frac{2}{3}\frac{\Delta\epsilon_{\rm nuc}r_{\rm burn}}{GMm_{\rm n}}\frac{r_{\rm burn}}{\Delta r_{\rm burn}}, \quad (22)$$

where we have used equation (12), neglecting terms $\propto (H/r)^2$.

Due to the temperature sensitivity of nuclear burning rates, $r = r_{\rm burn}$ generally occurs within a factor of $\lesssim 2$ of a fixed temperature $T = T_{\rm burn}$, which depends primarily just on the element under consideration. Because the radius and temperature of burning are related by

$$r_{\rm burn} \simeq \begin{cases} \dfrac{\mu GMm_{\rm n}}{kT_{\rm burn}}\left(\dfrac{H}{r}\right)^2, & P_{\rm gas} \gg P_{\rm rad}, \\ \left(\dfrac{\dot{M}G^{1/2}M^{1/2}}{2\pi\alpha a T_{\rm burn}^4}\dfrac{r}{H}\right)^{2/5}, & P_{\rm rad} \gg P_{\rm gas}, \end{cases} \quad (23)$$

in gas and radiation-dominated regimes, respectively, we can write

$$\left.\frac{\dot{q}_{\rm nuc}}{\dot{q}_{\rm visc}}\right|_{r=r_{\rm burn}} = \frac{H}{\Delta r_{\rm burn}} \times \begin{cases} 7.5\left(\dfrac{\Delta\epsilon_{\rm nuc}}{\rm MeV}\right)\left(\dfrac{T_{\rm burn}}{10^9\,{\rm K}}\right)^{-1}, & \dfrac{P_{\rm gas}}{P_{\rm rad}} \gg 1 \\ 3\left(\dfrac{\Delta\epsilon_{\rm nuc}}{\rm MeV}\right)\left(\dfrac{M}{1.4\,{\rm M}_\odot}\right)^{-0.8}\left(\dfrac{\alpha}{0.1}\right)^{-0.4} & \\ \quad\left(\dfrac{\dot{M}}{10^{-3}\,{\rm M}_\odot\,{\rm s}^{-1}}\right)^{0.4}\left(\dfrac{T_{\rm burn}}{10^9\,{\rm K}}\right)^{-1.6}, & \dfrac{P_{\rm rad}}{P_{\rm gas}} \gg 1 \end{cases}. \quad (24)$$

where we have assumed that $H/r = 0.4$ and a mean molecular weight $\mu = 2$. Assuming nominal gas pressure dominance, the ratio of radiation to gas pressure is given by

$$\frac{P_{\rm rad}}{P_{\rm gas}} \simeq 2\pi\alpha\mu^{5/2}m_{\rm p}^{5/2}k_{\rm b}^{-5/2}a_r(GM)^2\dot{M}^{-1}\left(\frac{H}{r}\right)^6 \approx 1\left(\frac{\alpha}{0.1}\right)\left(\frac{H/r}{0.4}\right)^6\left(\frac{M}{1.4\,{\rm M}_\odot}\right)^2\left(\frac{T_{\rm burn}}{10^9{\rm K}}\right)^{3/2} \times \left(\frac{\dot{M}}{10^{-3}\,{\rm M}_\odot\,{\rm s}^{-1}}\right)^{-1}. \quad (25)$$

Turbulent mixing likely sets a lower limit of $\Delta r_{\rm burn} \gtrsim H$ on the radial extent of burning. On the other hand, burning is unlikely to occur over a much larger radial region $\Delta r_{\rm burn} \gg r_{\rm burn} \sim 2H$ due to the sensitive temperature dependence of the nuclear reaction rates and the power-law behaviour of $T(r)$. The bracketed quantity in equation (24) is thus a reasonable estimate of $\dot{q}_{\rm nuc}/\dot{q}_{\rm visc}$. The approximate equality $\dot{q}_{\rm nuc} \gtrsim \dot{q}_{\rm visc}$ may be considered a loose definition for whether a disc is in the NuDAF regime on a radial scale $r \approx r_{\rm burn}$.

As an example, consider carbon burning ($Q/A \simeq 0.38$ MeV nucleon^{-1}; $T_{\rm burn} \approx 1.5 \times 10^9$ K) in a NS disc with a mass fraction $X_{12} = 0.5$, for which $\Delta\epsilon_{\rm nuc} \approx 0.2$ MeV. Equation (24) shows that $\dot{q}_{\rm nuc} \lesssim \dot{q}_{\rm visc}$ for $\dot{M} = 10^{-3}\,{\rm M}_\odot\,{\rm s}^{-1}$ and $\alpha = 0.1$, a result seemingly independent of $\dot{M}$ or the mass of the central object. However, this result holds only if gas pressure dominates [$\dot{M} \gtrsim 10^{-3}(\alpha/0.1)\,{\rm M}_\odot\,{\rm s}^{-1}$; equation 24]. At lower accretion rates, radiation pressure dominates, in which case $\dot{q}_{\rm nuc}/\dot{q}_{\rm visc}$ decreases $\propto \dot{M}^{0.4}M^{-0.8}$.

5 ELECTROMAGNETIC COUNTERPARTS

In this section we use our results from Section 4 to assess possible EM counterparts of WD–NS/BH mergers.

5.1 Gamma-ray burst

A previously discussed EM counterpart of WD–NS/BH mergers is a long-duration gamma-ray burst, powered by accretion on to the central BH (Fryer et al. 1999) or NS (King et al. 2007a). Although the formation of a relativistic jet from the inner disc is certainly possible, our calculations show that the accreted mass reaching the NS surface or BH event horizon may be a factor of $\sim$10–100 smaller than that of the original WD (although see Section 4.4). Among other things, this suggests that WD–NS mergers resulting in BH formation may be relatively rare.

Even if sufficient mass accretes to produce a powerful jet, only a small fraction of GRB jets are pointed towards the Earth. For off-axis events, the prompt and afterglow emission are much dimmer due

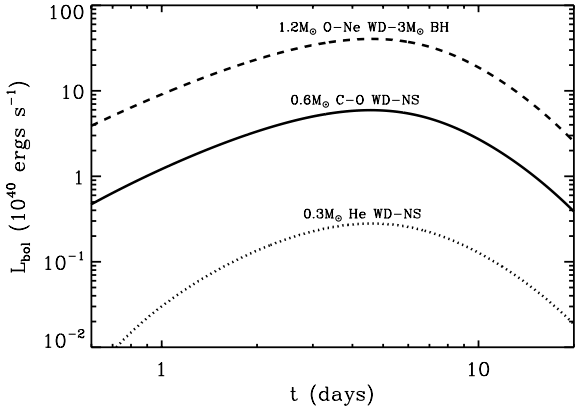

Figure 7. Bolometric light curve of supernova-like emission from WD–NS/BH mergers, powered by the decay of ^{56}Ni in the wind-driven ejecta. Three models shown correspond to the merger of (1) a $0.6\,M_\odot$ C–O WD with a $1.4\,M_\odot$ NS (solid; $\bar{v}_w \simeq 2.8\times10^4\,km\,s^{-1}$; $M_{ej}\simeq 0.5\,M_\odot$; $M_{Ni}=6\times10^{-3}\,M_\odot$; Fig. 2); (2) a $0.3\,M_\odot$ He WD with a $1.2\,M_\odot$ NS (dotted; $\bar{v}_w \simeq 2.2\times10^4\,km\,s^{-1}$; $M_{ej}\simeq 0.3\,M_\odot$; $M_{Ni}=3\times10^{-4}\,M_\odot$; Fig. 3) and (3) a $1.2\,M_\odot$ O–Ne WD with a $3\,M_\odot$ BH (dashed; $\bar{v}_w \simeq 4.6\times10^4\,km\,s^{-1}$; $M_{ej}\simeq 1\,M_\odot$; $M_{Ni}=5\times10^{-2}\,M_\odot$; Fig. 5).

to relativistic debeaming. Thus, although it would be unsurprising if WD–NS/BH mergers were accompanied by non-thermal jetted emission at some level, bright high-energy emission may not be a ubiquitous feature.

5.2 Radioactively powered optical transient

A promising source of isotropic EM emission from WD–NS/BH mergers is a SN-like transient, powered by the radioactive decay of ^{56}Ni from the wind-driven ejecta. We argued in Section 4.2 that outflows from the disc form a singular homologous 'shell' on large scales. Depending on the binary parameters and the wind efficiency η_w, the ejecta has a characteristic mass $M_{ej}\sim 0.3$–$1\,M_\odot$, mean velocity $\bar{v}_{ej}\approx 1$–$5\times10^4\,km\,s^{-1}$ and Ni mass $M_{Ni}\approx X_{56}M_{ej}\sim 10^{-4.5}$ to $10^{-2.5}\,M_\odot$ (Table 2). More massive WDs generally produce more massive ejecta, with a higher speed and larger Ni yield. This conclusion should be taken with caution, however; thermal instability may alter the disc evolution, especially for high mass (and possibly hybrid) WDs (Section 4.3).

Fig. 7 shows bolometric light curves of Ni decay-powered transients from WD–NS/BH mergers, calculated using the model of Kulkarni (2005) and Metzger, Piro & Quataert (2008b) for ejecta properties corresponding to different examples of WD–NS/BH systems from Section 4. In all cases the light curve peaks on a timescale $\sim$ week. By contrast, the peak luminosity L_{bol} varies from $\sim10^{39}$ to $10^{41.5}$ erg s^{-1} (absolute magnitude $M_B\simeq -9$ to -15), as results primarily from the large spread in ^{56}Ni mass, which depends primarily on the mass of the disrupted WD.

5.2.1 Comparison to observed subluminous Type I SN

At least in the case of C–O and O–Ne mergers, both the brightness and duration of the predicted transient are broadly consistent with the properties of recently discovered subluminous SNe I such as 2005E, 2008ha and 2010X (Section 1). On closer inspection, however, connecting individual events (or classes of events) to WD–NS/BH mergers results in several potential difficulties.

Although the ejecta mass, Ni mass and presence of C, O, Si, S, Ca, Fe from C–O/O–Ne WD mergers are all broadly consistent with the observed properties of SN 2008ha (Foley et al. 2009, 2010; Valenti et al. 2009), the velocity of the ejecta $\lesssim10^4\,km\,s^{-1}$ inferred for this and other '2002cx-like' events are much lower than the predictions of our baseline models. One caveat is that our calculations of $\bar{v}_{ej}$ assume that winds from all radii in the disc contribute to a single homologous body of ejecta, whereas in reality $\bar{v}_{ej}$ could be smaller if the fast wind from the inner disc escapes along the pole without efficiently coupling its kinetic energy.

The ejecta mass, Ni mass, velocity and presence of He, Ca and O of our C–O and He WD models are similarly consistent with the properties of SN 2005E. However, the large Ca mass $\gtrsim0.1\,M_\odot$ inferred in the ejecta of this and related events (Perets et al. 2010) is much higher than we predict. If this disagreement can be reconciled, we speculate that the mysterious location of 05E-like objects in the outskirts of their host galaxies could be explained by our model if WD–NS binaries are given a 'kick' during their supernova, which removes them from the disc of the galaxy by the time of merger.

For SN 2010X, again many of the elements produced by WD–NS/BH mergers are seen in the spectra (and some, like C and other intermediate-mass elements, are not expected in alternative .Ia models; Kasliwal et al. 2010). However, Ti is also observed, despite its low predicted quantity in our models. Furthermore, none of our models produces enough ^{56}Ni to explain SN 2002bj (Poznanski et al. 2010), an event which otherwise shares several properties with 2010X. Again, these conclusions must be moderated due to our ignorance of the outcome of high mass ratio mergers and the uncertain effects of thermal instabilities.

As a final note, although this possibility has been neglected thus far, free nucleons from the very inner disc may also contribute a small fraction of the ejected mass (Fig. 1). These may be lost to winds heated by viscous dissipation (as discussed here) or by neutrino irradiation from the very inner disc or boundary layer (e.g. Metzger, Thompson & Quataert 2008a; Metzger, Piro & Quataert 2008b). Once neutrons decay, the net effect is contamination of the ejecta with hydrogen. Since even a small quantity of H may be detectable due to its strong lines, its presence in an event otherwise classified 'Type I' would support the WD–NS/BH merger model, due to its unlikely presence in other WD models (its absence would, however, not rule out the model).

5.3 Radio transients

A final source of transient emission from WD–NS/BH mergers is non-thermal synchrotron emission powered by the deceleration of the ejecta with the surrounding interstellar medium (ISM). Shock emission peaks once the ejecta sweeps up its own mass in the ISM; this occurs on a time-scale

$$t_{dec}\approx 10\left(\frac{M_{ej}}{0.3\,M_\odot}\right)^{1/3}\left(\frac{\bar{v}_{ej}}{10^4\,km\,s^{-1}}\right)^{-1}\left(\frac{n}{cm^{-3}}\right)^{-1/3}\,yr, \quad (26)$$

where n is the ISM density. Following Nakar & Piran (2011) (their equation 14), we estimate that the number of radio transients detectable with a single 1.4-GHz snapshot of the whole sky down to a limiting flux F_{lim} is given by

$$N_{1.4}\approx 10\left(\frac{M_{ej}}{0.3\,M_\odot}\right)^{1.8}\left(\frac{\bar{v}_{ej}}{10^4 km\,s^{-1}}\right)^{6.1}\left(\frac{n}{cm^{-3}}\right)\left(\frac{\epsilon_B}{0.1}\right)^{1.3}$$
$$\times\left(\frac{\epsilon_e}{0.1}\right)^{2.3}\left(\frac{F_{lim}}{0.1\,mJy}\right)^{-1.5}\left(\frac{\mathcal{R}}{10^{-4}\,yr^{-1}}\right), \quad (27)$$

where $\mathcal{R}\sim10^{-5}$ to $10^{-3}\,yr^{-1}$ is the merger rate per galaxy (see Section 2) and we have assumed that relativistic electrons are accelerated into a power-law energy distribution with index $p=2.5$.

Here $\epsilon_e(\epsilon_B)$ are the fraction of the energy density behind the shock imparted to relativistic electrons and magnetic fields, respectively, normalized to values characteristic of radio supernovae (Chevalier 1998). Equations (26) and (27) show that future wide-field radio surveys at ∼GHz frequencies (e.g. Bower et al. 2010) will preferentially detect those events with the highest ejecta mass and velocity, as characterized by higher mass WD mergers in our model. This is due both to the sensitive dependence of $N_{1.4}$ on $M_{\rm ej}$ and $\bar{v}_{\rm ej}$ and the requirement that $t_{\rm dec}$ be sufficiently short to produce an appreciable change in the radio brightness over the characteristic lifetime of the survey.

6 DISCUSSION AND CONCLUSIONS

Although the effects of nuclear burning on accretion have been explored in previous work (e.g. Taam & Fryxell 1985; Chakrabarti, Jin & Arnett 1987), these efforts focused on systems with much lower accretion rates, such as X-ray binaries. Unphysically low values of the disc viscosity $\alpha \lesssim 10^{-10}$ are necessary in these cases to achieve sufficiently high densities for appreciable nucleosynthesis. Here we have shown that nuclear burning has an important effect on the *dynamics* of accretion following the tidal disruption of a WD by a NS or stellar mass BH, even for more realistic values of $\alpha \gtrsim 0.01$–0.1. Under conditions when the heating from nuclear burning is comparable to, or greater than that, released by viscous dissipation, we have introduced the concept of a 'NuDAF' (see the discussion surrounding equation 24 for a more concrete definition of this regime). The dependence of the disc thermodynamics on nuclear burning is particularly acute because inflow is already radiatively inefficient and hence marginally bound (Narayan & Yi 1994), even without an additional heat source.

In Section 5 we discussed several sources of transient emission associated with WD–NS/BH mergers. In addition to their EM signatures, WD–NS/BH binaries are considered a promising source of gravitational wave emission at frequencies $\lesssim$mHz. Estimates suggest that a space-based interferometer such as *LISA* could resolve ∼1–100 WD–NS/BH systems within our Galaxy (Nelemans, Yungelson & Portegies Zwart 2001; Cooray 2004; Paschalidis et al. 2009). Unfortunately, most of the discovered systems will require $\gtrsim 10^4$ years to merge. Although the odds are not favourable, if a WD–NS/BH binary in the Milky Way or a nearby galaxy were sufficiently compact to merge on a shorter time-scale, it should be relatively easy to detect and localize. EM counterpart searches could then be triggered at the expected merger time.

The results presented here may be applied to other contexts. One immediate possibility is the tidal disruption of a WD by an intermediate-mass BH (e.g. Rosswog, Ramirez-Ruiz & Hix 2009; Clausen & Eracleous 2011). For nearly circular orbits prior to merger (as we have discussed), burning is unlikely to be important if the primary mass M is too large. This is because when radiation pressure dominates (as is likely in this case; equation 25), the ratio of nuclear to viscous heating $\dot{q}_{\rm nuc}/\dot{q}_{\rm visc} \propto M^{-0.8}$ (equation 24) is small due to the deep potential well of the BH. On the other hand, for highly elliptical orbits with small pericentre radii, tidal forces during the disruption can themselves trigger a nuclear runaway (Rosswog et al. 2009); because the initial orbit has a very low binding energy, the nuclear energy released will have a more significant effect on what matter is unbound.

A possibly more direct application of our results is to accretion following the core collapse of a massive star, as in the 'collapsar' model for long-duration GRBs (MacFadyen & Woosley 1999). Notably, the outer layers of the Wolf–Rayet progenitors of long GRBs are predicted to have a He–C–O composition (Woosley & Heger 2006), similar to that of a 'hybrid' WD (Fig. 4). Due to its low temperature threshold, the reaction $^4{\rm He} + {}^{16}{\rm O} \rightarrow {}^{20}{\rm Ne} + \gamma$ may have a particularly important influence on the disc, if material circularizes at a sufficiently large radius. Note that current numerical simulations of collapsar discs generally neglect the effects of nuclear reactions, except perhaps at very high temperature $\gtrsim 4 \times 10^9$ K (MacFadyen & Woosley 1999; Lindner et al. 2010; Milosavljevic et al. 2010). Our results show that this assumption may not be valid, as nuclear energy generation can be important, even for temperatures as low as $\sim 10^9$ K. The effects of nuclear burning may be similarly important in accretion following the merger of a helium star with a NS or BH (Fryer & Woosley 1998). The recent GRB 101225A was interpreted as resulting from accretion following following NS–helium star merger (Thöne et al. 2011); we note that the small Ni mass inferred from the weak SN associated with this event is consistent with our estimated yield from He WD–NS mergers.

There is much room for improvement on the model presented here in future work. As one example, we have assumed a time-steady, height-integrated disc model. In reality, the disc may have a complex vertical structure, due in part to the interplay between MRI-driven turbulence and convection, the latter driven by the strong temperature dependence of nuclear heating. Complex time-dependent behaviour is also expected, associated with both the secular viscous evolution of the disc and, potentially, shorter time-scale variability associated with thermal instability (possibly resulting in limit cycle behaviour; Section 4.3). We have assumed a simple outflow model with two uncertain parameters, $\eta_{\rm w}$ and ${\rm Be}'_{\rm d}$, whose values depend on the mechanism and heating source responsible for driving outflows from the disc corona. The pressure dependence of wind cooling has important implications for the thermal stability of the disc (Section 4.3). Our calculations also neglect the effects of convection on energy and angular momentum transport in the disc (Section 4.4), which, if important, could substantially increase the accretion time-scale or even alter the radial structure of the accreting envelope. Even our simple model cannot be directly applied to the merger of massive WDs with NSs, since nuclear burning is already important during the disc's formation itself. Here, multidimensional numerical simulations that include the effects of nuclear reactions will be required to fully characterize the evolution and fate of these systems.

Finally, the discussion of optical and radio EM counterparts in Sections 5.2 and 5.3 was necessarily limited in scope. In future work we will pursue more detailed calculations of the predicted optical light curve and spectra, as will be necessary to more precisely compare the predictions of our model to observations of subluminous SNe I (Section 5.2.1). This work will also address the expected detection rates with current and upcoming optical and radio transient surveys, given the current constraints on the merger rates of different WD–NS/BH systems.

ACKNOWLEDGMENTS

I thank J. Goodman for many helpful conservations and for encouraging my work on this topic, as well as for a thorough reading of the text. I thank C. Kim and D. Lorimer for helpful information on WD–NS binaries. I also thank D. Giannios, E. Quataert, R. Narayan, A. Piro, R. Foley, M. Kasliwal and L. Bildsten for helpful conversations and information. I thank F. Timmes for making his nuclear reaction codes available to the public. BDM is supported by NASA through Einstein Postdoctoral Fellowship grant number PF9-00065

awarded by the Chandra X-ray Center, which is operated by the Smithsonian Astrophysical Observatory for NASA under contract NAS8-03060.

REFERENCES

Bailes M., Ord S. M., Knight H. S., Hotan A. W., 2003, ApJ, 595, L49
Begelman M. C., Rossi E. M., Armitage P. J., 2008, MNRAS, 387, 1649
Bildsten L., Shen K. J., Weinberg N. N., Nelemans G., 2007, ApJ, 662, L95
Blandford R. D., Begelman M. C., 1999, MNRAS, 303, L1
Bower G. C. et al., 2010, ApJ, 725, 1792
Branch D., Baron E., Thomas R. C., Kasen D., Li W., Filippenko A. V., 2004, PASP, 116, 903
Cannizzo J. K., 1993, ApJ, 419, 318
Carballido A., Stone J. M., Pringle J. E., 2005, MNRAS, 358, 1055
Chakrabarti S. K., Jin L., Arnett W. D., 1987, ApJ, 313, 674
Chen W.-X., Beloborodov A. M., 2007, ApJ, 657, 383
Chevalier R. A., 1998, ApJ, 499, 810
Clausen D., Eracleous M., 2011, ApJ, 726, 34
Cooray A., 2004, MNRAS, 354, 25
D'Souza M. C. R., Motl P. M., Tohline J. E., Frank J., 2006, ApJ, 643, 381
Davies M. B., Ritter H., King A., 2002, MNRAS, 335, 369
Davis S. W., Stone J. M., Pessah M. E., 2010, ApJ, 713, 52
Edwards R. T., Bailes M., 2001, ApJ, 547, L37
Eggleton P. P., 1983, ApJ, 268, 368
Foley R. J. et al., 2009, AJ, 138, 376
Foley R. J., Brown P. J., Rest A., Challis P. J., Kirshner R. P., Wood-Vasey W. M., 2010, ApJ, 708, L61
Freire P., Wex N., 2010, arXiv:1006.0642
Fryer C. L., Woosley S. E., 1998, ApJ, 502, L9
Fryer C. L., Woosley S. E., Herant M., Davies M. B., 1999, ApJ, 520, 650
Guerrero J., García-Berro E., Isern J., 2004, A&A, 413, 257
Gutiérrez J., Canal R., García-Berro E., 2005, A&A, 435, 231
Han Z., Tout C. A., Eggleton P. P., 2000, MNRAS, 319, 215
Hawley J. F., Balbus S. A., 2002, ApJ, 573, 738
Hawley J. F., Balbus S. A., Stone J. M., 2001, ApJ, 554, L49
Iben I., Jr, Tutukov A. V., 1991, ApJ, 370, 615
Igumenshchev I. V., Abramowicz M. A., Narayan R., 2000, ApJ, 537, L27
Jha S., Branch D., Chornock R., Foley R. J., Li W., Swift B. J., Casebeer D., Filippenko A. V., 2006, AJ, 132, 189
Kaiser N. et al., 2002, in Tyson J. A., Wolff S., eds, Proc. SPIE Conf. Ser. Vol. 4836, Pan-STARRS: A Large Synoptic Survey Telescope Array. SPIE, Bellingham, p. 154
Kasliwal M. M. et al., 2010, ApJ, 723, L98
Kaspi V. M. et al., 2000, ApJ, 543, 321
Kim C., Kalogera V., Lorimer D. R., White T., 2004, ApJ, 616, 1109
King A., Olsson E., Davies M. B., 2007a, MNRAS, 374, L34
King A. R., Pringle J. E., Livio M., 2007b, MNRAS, 376, 1740
Kohri K., Narayan R., Piran T., 2005, ApJ, 629, 341
Kulkarni S. R., 2005, arXiv:astro-ph/0510256
Lamers H. J. G. L. M., Cassinelli J. P., 1999, Introduction to Stellar Winds. Cambridge Univ. Press, Cambridge
Laughlin G., Bodenheimer P., 1994, ApJ, 436, 335
Law N. M. et al., 2009, PASP, 121, 1395
Li W. et al., 2003, PASP, 115, 453
Lindner C. C., Milosavljević M., Couch S. M., Kumar P., 2010, ApJ, 713, 800
Livne E., Arnett D., 1995, ApJ, 452, 62
Lorimer D. R., 2005, Living Rev. Relativ., 8, 7
Lundgren S. C., Zepka A. F., Cordes J. M., 1995, ApJ, 453, 419
MacFadyen A. I., Woosley S. E., 1999, ApJ, 524, 262
Metzger B. D., Thompson T. A., Quataert E., 2008a, ApJ, 676, 1130
Metzger B. D., Piro A. L., Quataert E., 2008b, MNRAS, 390, 781
Milosavljevic M., Lindner C. C., Shen R., Kumar P., 2010, arXiv:1007.0763
Moriya T., Tominaga N., Tanaka M., Nomoto K., Sauer D. N., Mazzali P. A., Maeda K., Suzuki T., 2010, ApJ, 719, 1445
Nakar E., Piran T., 2011, Nat, 478, 82
Narayan R., Yi I., 1994, ApJ, 428, L13
Narayan R., Yi I., 1995, ApJ, 444, 231
Narayan R., Mahadevan R., Quataert E., 1998, in Abramowicz M. A., Bjornsson G., Pringle J. E., eds, Theory of Black Hole Accretion Disks. Cambridge Univ. Press, Cambridge, p. 148
Narayan R., Igumenshchev I. V., Abramowicz M. A., 2000, ApJ, 539, 798
Narayan R., Piran T., Kumar P., 2001, ApJ, 557, 949
Narayan R., Quataert E., Igumenshchev I. V., Abramowicz M. A., 2002, ApJ, 577, 295
Nauenberg M., 1972, ApJ, 175, 417
Nelemans G., Yungelson L. R., Portegies Zwart S. F., 2001, A&A, 375, 890
Nomoto K., Thielemann F.-K., Yokoi K., 1984, ApJ, 286, 644
O'Shaughnessy R., Kim C., 2010, ApJ, 715, 230
Ohsuga K., Mori M., Nakamoto T., Mineshige S., 2005, ApJ, 628, 368
Paschalidis V., MacLeod M., Baumgarte T. W., Shapiro S. L., 2009, Phys. Rev. D, 80, 024006
Perets H. B. et al., 2010, Nat, 465, 322
Perets H. B., Badenes C., Arcavi I., Simon J. D., Gal-yam A., 2011, ApJ, 730, 89
Phillips M. M. et al., 2007, PASP, 119, 360
Piran T., 1978, ApJ, 221, 652
Portegies Zwart S. F., Yungelson L. R., 1999, MNRAS, 309, 26
Poznanski D. et al., 2010, Sci, 327, 58
Quataert E., Gruzinov A., 2000, ApJ, 539, 809
Rau A. et al., 2009, PASP, 121, 1334
Rosswog S., Ramirez-Ruiz E., Hix W. R., 2009, ApJ, 695, 404
Ryu D., Goodman J., 1992, ApJ, 388, 438
Salaris M., Dominguez I., Garcia-Berro E., Hernanz M., Isern J., Mochkovitch R., 1997, ApJ, 486, 413
Shakura N. I., Sunyaev R. A., 1973, A&A, 24, 337
Shen K. J., Kasen D., Weinberg N. N., Bildsten L., Scannapieco E., 2010, ApJ, 715, 767
Sigurdsson S., Rees M. J., 1997, MNRAS, 284, 318
Taam R. E., Fryxell B. A., 1985, ApJ, 294, 303
Tauris T. M., Sennels T., 2000, A&A, 355, 236
Thompson T. A., 2010, arXiv:1011.4322
Thöne C. C. et al., 2011, arXiv:1105.3015
Thorne K. S., Zytkow A. N., 1975, ApJ, 199, L19
Timmes F. X., 1999, ApJS, 124, 241
Valenti S. et al., 2009, Nat, 459, 674
van den Heuvel E. P. J., Bonsdema P. T. J., 1984, A&A, 139, L16
Verbunt F., Rappaport S., 1988, ApJ, 332, 193
Verbunt F., van den Heuvel E. P. J., 1995, in Lewin W. H. G., van Paradijs J., van den Heuvel E. P. J., eds, X-ray Binaries. Astronomisches Rechen-Institut, Heidelberg, p. 457
Waldman R., Sauer D., Livne E., Perets H., Glasner A., Mazzali P., Truran J. W., Gal-Yam A., 2011, ApJ, 738, 21
Woosley S. E., Heger A., 2006, ApJ, 637, 914
Woosley S. E., Kasen D., 2011, ApJ, 734, 38
Woosley S. E., Taam R. E., Weaver T. A., 1986, ApJ, 301, 601
Yungelson L. R., Nelemans G., van den Heuvel E. P. J., 2002, A&A, 388, 546

This paper has been typeset from a TEX/LATEX file prepared by the author.